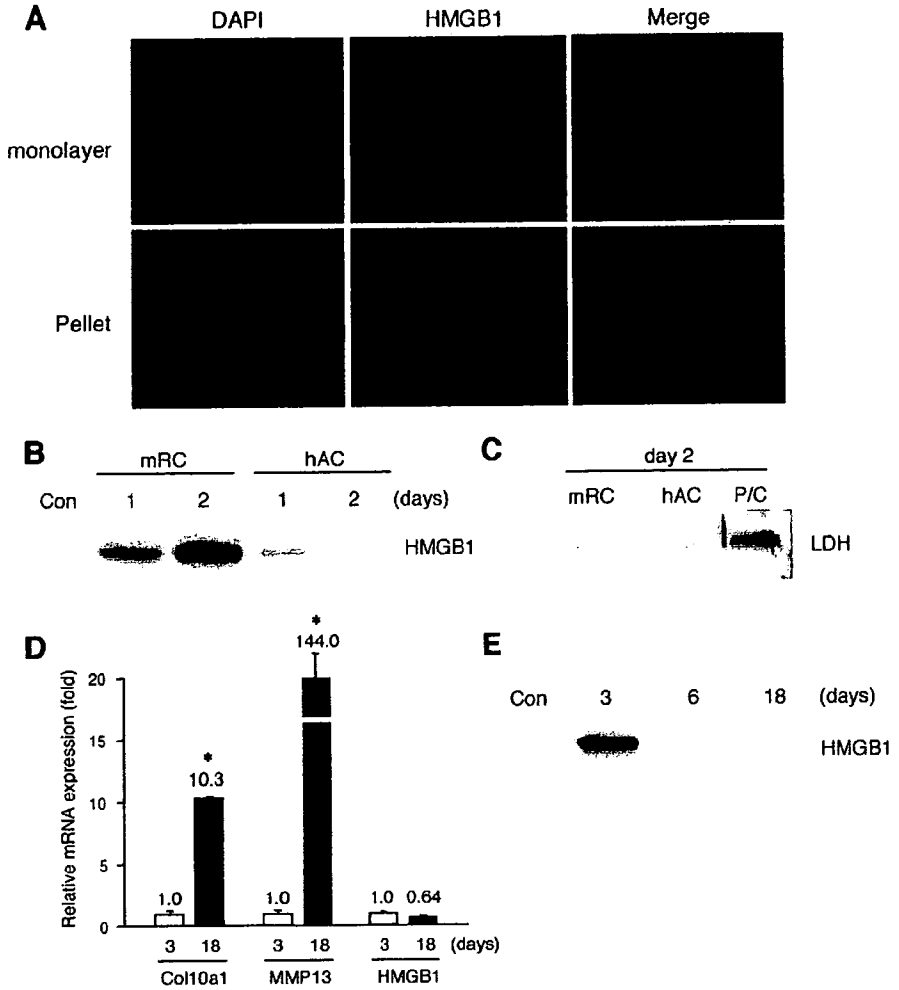

FIG. 8. HMGB1 release from differentiating cultured rib chondrocytes. (A) Immunofluorescence assay shows that monolayer rib chondrocytes isolated from the ventral parts of mice rib cartilage express HMGB1 only in the nucleus, whereas in pelleted rib chondrocytes cultured for 2 days HMGB1 is localized in the cytosol. The extracellular release of HMGB1 was verified with immunoblotting. (B) HMGB1 was determined in the supernatant of pelleted mice rib chondrocytes (mRC) on days 1 and 2, whereas human articular chondrocytes (hAC) do not release HMGB1 in pellet culture. (C) Immunoblotting with LDH antibody shows that this secretion is independent of necrotic cell death. The positive control (P/C) is the same sample as shown in Fig. 7G. (D) During the culture of pelleted mRC for 18 days, quantitative PCR demonstrates that the mRNA level of cartilage maturation markers such as Col10a1 and MMP13 increases significantly on day 18, although that of HMGB1 is unchanged. (E) Only the supernatant on day 3 contains HMGB1. Statistically significant differences from mRNA expression on day 3 are indicated, respectively (*, $P < 0.01$).

Osteogenesis in *Hmgb1*$^{-/-}$ mice. As shown in Fig. 1, *Hmgb1*$^{-/-}$ forelimbs appeared to be reduced in size and calcification and were abnormally bent or fractured. Since these findings suggest a reduction of bone mineralization, we investigated osteoblast differentiation in *Hmgb1*$^{-/-}$ bones. Using von Kossa staining, we found that calcified cartilage had progressed to bone marrow in the radii and ulnas of wild-type mice (Fig. 6A) but not in *Hmgb1*$^{-/-}$ mice (Fig. 6B). Osteopontin, a hypertrophic cartilage marker as well as an osteoblast marker (35), was strongly expressed in the calcified hypertrophic cartilage of *Hmgb1*$^{-/-}$ bones (Fig. 6D) in which Col1a1-positive cells, an early marker of osteoblast differentiation (18), were not found; these cells were accumulated at the collar surrounding the growth plate (Fig. 6F). In contrast, Col1a1-positive cells were widely distributed in the bone marrow of wild-type mice (Fig. 6E), suggesting that osteoblast invasion was suppressed in *Hmgb1*$^{-/-}$ limbs. The essential transcription factors for osteoblast differentiation, Runx2 (27) and Osterix (34), were highly expressed in the primary ossification center of the wild-type radius (Fig. 6G and I), whereas they were barely detectable in the *Hmgb1*$^{-/-}$ bones (Fig. 6H and J). Osteocalcin, which is thought to be a terminal marker for osteoblastic maturation (29), was found at the periphery of hypertrophic cartilage in *Hmgb1*$^{-/-}$ bones at E16.5 (Fig. 6L); however, it appeared in the bone marrow at E17.5 (data not shown) rather than at E16.5 as in wild-type mice (Fig. 6K). Thus, the delay in primary ossification of *Hmgb1*$^{-/-}$ hypertrophic cartilage was coupled to a delay in recruitment of osteoblasts, suggesting that subsequent osteoblastic differentiation progressed similarly in wild-type and *Hmgb1*$^{-/-}$ mice.

HMGB1 is released from differentiating cartilage in organ culture. To examine the secretion of HMGB1 from chon-

Downloaded from mcb.asm.org by on April 3, 2008

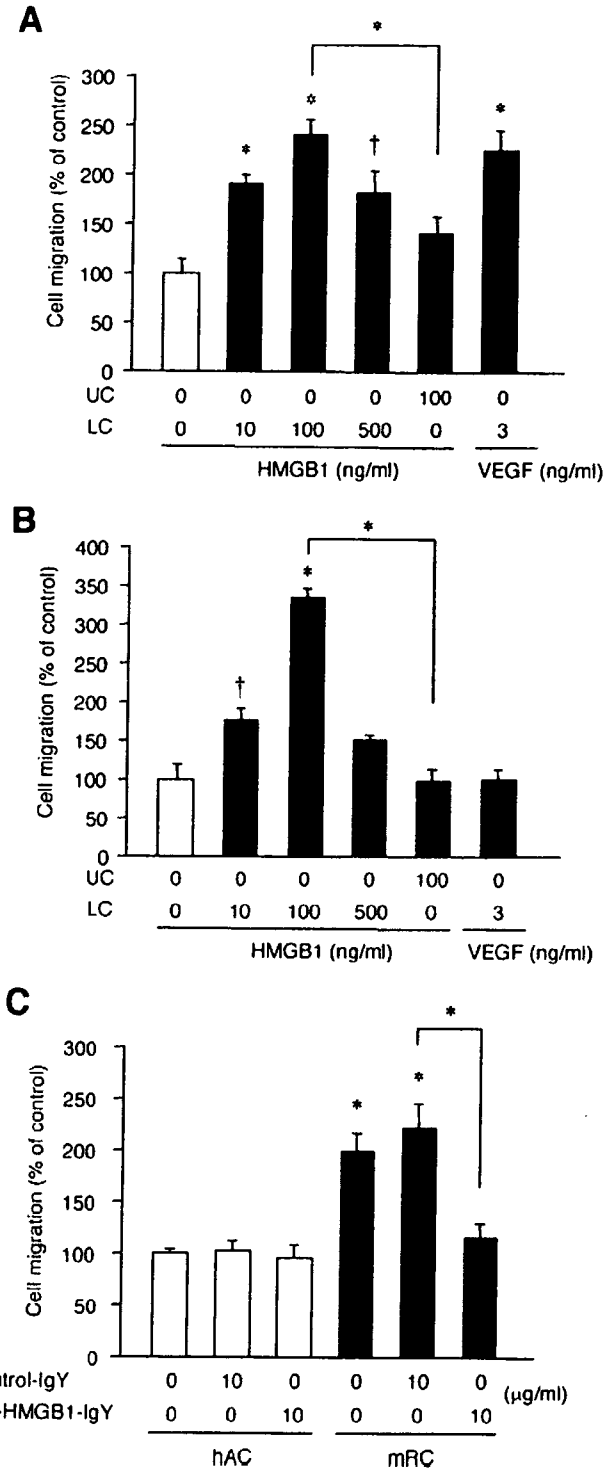

FIG. 9. Chondrocyte-secreted HMGB1 is a chemoattractant for osteoclasts. The chemotactic effect of recombinant HMGB1 on osteoclasts was examined by Boyden chambers with or without addition of HMGB1 to either the lower chamber (LC) or the upper chamber (UC) as indicated. (A) HMGB1 recruits osteoclasts at 10 ng/ml, and efficacy peaks at 100 ng/ml. The addition of HMGB1 to the upper chamber does not significantly activate osteoclast invasion. (B) HMGB1 also recruits osteoblastic MC3T3-E1 cells with a tendency similar to that described above, although VEGF does not. Statistically significant differences from control migrations without added chemoattractants are indicated, respectively (*, $P < 0.01$; †, $P < 0.05$). (C) Chemotaxis assay using the supernatant of pelleted mice rib chondrocytes (mRC) and human articular chondrocytes (hAC) after 3 days culture. The supernatant of hAC does not recruit osteoclasts, whereas that of mRC attracts osteoclasts significantly, and this effect is abrogated by addition of anti-HMGB1 IgY. Cell migration is shown as mean ± the standard deviation of four replicates. Statistically significant differences from control migrations by the supernatant of hAC are indicated (*, $P < 0.01$).

drocytes, we used the cartilage organ culture system (20). Metatarsal bones were isolated from embryos at E15.5 and cultured in conditioned medium for up to 5 days. Immunohistochemistry revealed that HMGB1 was localized in hypertrophic chondrocytes on day 2 (Fig. 7A) and that expression was attenuated on day 5 (Fig. 7B). Von Kossa staining of the adjacent sections indicated that this expression occurred in hypertrophic cartilage and not in calcified cartilage (Fig. 7C and D). Using immunoblotting, we determined that HMGB1 was present in the supernatant, with a peak 3 days after the start of organ culture, and then it decreased (Fig. 7E), showing that HMGB1 was released into the medium by hypertrophic chondrocytes. This result was reproduced with a large long bone, the tibia, which was isolated from the embryos at E14.5 (Fig. 7F). Immunoblotting with LDH antibody was negative, indicating that HMGB1 was actively secreted and not released passively as a consequence of necrotic cell death (Fig. 7G). Using ELISA, we quantified the HMGB1 protein released into the medium of tibia organ culture and found that it peaked on days 3 through 5 at concentrations of >10 ng/ml (Fig. 7H).

HMGB1 is released specifically from hypertrophic chondrocytes. It has been previously demonstrated that HMGB1 is released from osteoclasts and osteoblast-like cells (12, 42). To prove that the release of HMGB1 into the supernatant was from chondrocytes in organ culture, we used pellet cultures of rib growth plate chondrocytes, since this culture system mimics in vivo cartilage differentiation (5). Monolayer chondrocytes isolated from the ventral parts of mouse rib cartilage expressed HMGB1 only in the nucleus; however, when cultured as differentiating cell pellets, HMGB1 was localized in the cytosol (Fig. 8A). Extracellular HMGB1 was detected in the supernatant of pelleted rib chondrocytes on days 1 and 2; in contrast, articular chondrocytes, which do not differentiate to hypertrophic cartilage under the three-dimensional condition such as pellet or alginate culture (6, 40), did not release HMGB1 (Fig. 8B). Immunoblotting with LDH antibody showed that HMGB1 release was not caused by necrotic cell death (Fig. 8C). In addition, to examine HMGB1 expression in longer-term cultures, we maintained the rib chondrocyte pellets for 18 days. Quantitative PCR demonstrated that mRNA of cartilage maturation markers such as Col10a1 and MMP13 increased significantly, showing that chondrocyte differentiation had occurred (Fig. 8D). Only the medium from day 3 contained HMGB1 (Fig. 8E), although the mRNA level of HMGB1 did not significantly change between day 3 and 18. These results indicate that HMGB1 is secreted during the early phase of cartilage maturation.

HMGB1 is a chemoattractant for osteoclasts and osteoblasts. As we showed in Fig. 4, 5, and 6, *Hmgb1*$^{-/-}$ embryos

Downloaded from mcb.asm.org by on April 3, 2008

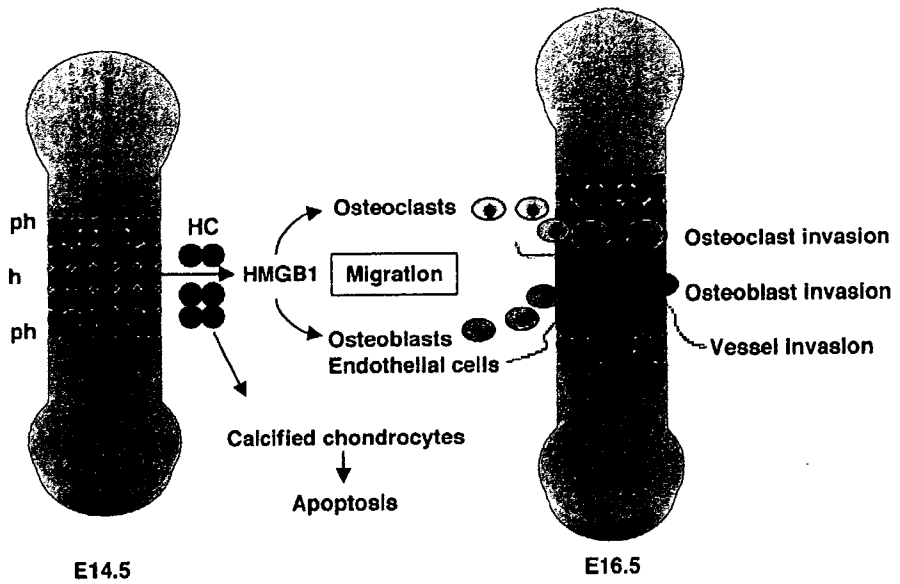

FIG. 10. Role of HMGB1 in skeletal development. During endochondral ossification, a region of resting chondrocytes transforms into a zone of proliferating chondrocytes that then undergo hypertrophy and subsequently apoptosis. HMGB1 is released from the hypertrophic chondrocytes just before undergoing programmed cell death; it acts as an extracellular signal for the migration of osteoclasts, osteoblasts, and endothelial cells that replace cartilage with bone and bone marrow. ph, prehypertrophic cartilage; h, hypertophic cartilage; bm, bone marrow; HC, hypertrophic chondrocytes.

were defective in invasion by TRAP- and Col1a1-positive cells, as well as CD31-positive cells, at the primary ossification center. Since HMGB1 has chemotactic effects on endothelial cells (32, 46), we tested for similar effects on osteoclasts and osteoblasts. Recombinant HMGB1 at 10 ng/ml recruited osteoclasts in Boyden chambers, and peak migration occurred at 100 ng/ml; this level of efficacy was similar to that of VEGF used as a positive control (22) (Fig. 9A). Addition of HMGB1 to the upper chamber did not significantly activate osteoclast migration. HMGB1 also induced chemotaxis for MC3T3-E1 osteoblast-like cells with a tendency similar to that described above (Fig. 9B), although VEGF did not (16). These findings suggest that osteoclast and osteoblast invasion at the primary ossification center might be a direct effect of HMGB1-induced chemoattraction.

Finally, we investigated whether HMGB1 released by differentiating chondrocytes could promote osteoclast migration. Using the supernatant of pelleted rib chondrocytes and articular chondrocytes cultured for 3 days (see Fig. S2 in the supplemental material), we compared the chemotactic effect for osteoclasts. The supernatant of articular chondrocytes did not recruit osteoclasts; however, the supernatant of rib chondrocytes attracted osteoclasts significantly, and the effect was abrogated by neutralizing anti-HMGB1 IgY (Fig. 9C). This result supports our hypothesis that differentiating chondrocytes could regulate cell migration directly via HMGB1 secretion.

DISCUSSION

This study demonstrates that the stage-specific secretion of HMGB1 in cartilage regulates endochondral ossification, at least in part, by acting as a chemotactic factor for osteoclasts and osteoblasts, as well as endothelial cells. We examined skeletal development in *Hmgb1*$^{-/-}$ embryos and found significant alterations in the bones formed by endochondral ossification, whereas calvariae, which are formed by intramembranous ossification, were somewhat misshapen; but the effect was slight, and the cartilage formation was not affected. The analysis of *Hmgb1*$^{-/-}$ limb sections revealed that the onset of cartilage differentiation was similar in *Hmgb1*$^{-/-}$ and wild-type embryos; however, the invasion of TRAP- and Col1a1-positive cells, as well as CD31-positive cells, into the primary ossification center was remarkably impaired in *Hmgb1*$^{-/-}$ limbs. Thus, the *Hmgb1*$^{-/-}$ growth plates are strikingly lengthened and deficient in osteoblast and osteoclast invasion as well as vascularization, which may result in weak bones that can bend or fracture.

To examine the expression of HMGB1 in developing limbs, we used in situ hybridization: HMGB1 mRNA expression was ubiquitous in the cells of all zones of the growth plate from E14.5 through E16.5 (data not shown). In contrast, HMGB1 protein was present in the nuclei of prehypertrophic chondrocytes in tibia at E14.5 and in the cytosol of hypertrophic chondrocytes at E15.5 but was not detectable in resting and proliferating chondrocytes. The active secretion of HMGB1 from chondrocytes was verified with organ culture and pellet culture systems; we found that HMGB1 was translocated from the nucleus to the cytosol and actively secreted at the early phase of chondrocyte differentiation, but the secretion ceased at the late phase. Interestingly, secretion from pelleted rib chondrocytes occurred actively without added any stimulatory factor, whereas articular chondrocytes did not release HMGB1 in pellet culture. Chondrocyte-secreted HMGB1 was sufficient to chemoattract osteoclasts and osteoblasts, as well as endothelial cells as previously shown by others (32, 46). These findings suggest that HMGB1 released from hypertrophic chondrocytes may regulate skeletal development by controlling cell invasion

Downloaded from mcb.asm.org by on April 3, 2008

into the growth plate. At present, however, a potential role of HMGB1 as a nuclear factor, which is its other function, still remains possible in the developing cartilage.

Secretion of HMGB1 during specific stages of cell differentiation is not unique to chondrocytes and has been reported for dendritic cells (14) and neonatal rat type I astrocytes (41), although the mechanism of HMGB1 secretion during cell differentiation has yet to be elucidated. Thus far, Bonaldi et al. have reported that HMGB1 contains two nuclear localization signals (NLSs), and the acetylation of both NLSs is involved in the transport from the nucleus to the cytosol (8). Furthermore, HMGB1 can be phosphorylated, and the direction of transport is regulated by phosphorylation of both NLS regions (58). These findings suggest that HMGB1 release is independent from RNA expression and protein synthesis, which is compatible with our data showing that HMGB1 mRNA levels do not change in chondrocyte pellet cultures, despite its secretion.

The inhibition of the interaction between HMGB1 and the receptor for advanced glycation end products (RAGE), which is a specific receptor for HMGB1, suppresses the tumor proliferation, metastatic invasion, and expression of MMPs (48). RAGE is expressed in osteoclasts, osteoblasts (12), and endothelial cells (9), suggesting that RAGE might be associated with cell invasion during endochondral ossification; however, an analysis of *Rage*$^{-/-}$ mice (1) showed no alteration in skeletal development during embryogenesis (see Fig. S1B in the supplemental material). Moreover, *Rage*$^{-/-}$ mice manifest increased bone mass and bone mineral density and decreased bone resorptive activity due to a defect in osteoclast function (60). In our hands, however, MMP9 mRNA levels in calvariae at E18.5 were similar between wild-type and *Hmgb1*$^{-/-}$ mice (see Fig. S3A in the supplemental material), and MMP9-positive cells emerged in the bone marrow of developing limbs of both types of mice at E18.5 (see Fig. S3B in the supplemental material). The evidence that HMGB1-RAGE interaction is sufficient but not necessary for mesoangioblast migration (38) is a precedent for the idea that RAGE may not be the key receptor for HMGB1-induced cell recruitment at the primary ossification center. Additional HMGB1 receptors have been identified, including Toll-like receptors 2 and 4 (39), which appear in osteoclasts, osteoblasts, and endothelial cells (26, 49, 50), and syndecan (43), which is expressed in osteoblasts (24).

Our results indicate that HMGB1 might be important not only for tissue repair after injury but also for the organization of bone and cartilage development in the embryo. In endochondral ossification, a region of resting chondrocytes transforms into a zone of proliferating chondrocytes that then undergo hypertrophy and subsequently apoptosis (37). HMGB1 release from the hypertrophic cartilage occurs just before programmed cell death (Fig. 10), suggesting that HMGB1 may be an extracellular signal released from the tissue to be replaced (cartilage) toward the cells of new tissue to be formed (bone and bone marrow).

ACKNOWLEDGMENTS

We are grateful to Yasuhiko Kawakami and Thiennu Vu for helpful discussions; Kim Henriksen, Noriyuki Namba, and Chisa Shukunami for technical advice; Yasuhiko Yamamoto and Hiroshi Yamamoto for providing *Rage*$^{-/-}$ mice; and Shingo Yamada for providing the neutralizing anti-HMGB1 IgY and ELISA kit. We especially thank Lilo Creighton for her excellent immunohistochemical technique.

This study was supported by grants from the NIH (AR47360, AR50631, and AG07996), NIBI (ID05-24), Arthritis Foundation, JST SORST, Genome Network Project (MEXT), and Grants-in Aid for Scientific Research (MEXT) (H.A.) and a postdoctoral fellowship of the Japan Research Foundation for Clinical Pharmacology and Research Grant for Rheumatology Disease, Japan Rheumatism Foundation (N.T.).

REFERENCES

1. **Abeyama, K., D. M. Stern, Y. Ito, K. Kawahara, Y. Yoshimoto, M. Tanaka, T. Uchimura, N. Ida, Y. Yamazaki, S. Yamada, Y. Yamamoto, H. Yamamoto, S. Iino, N. Taniguchi, and I. Maruyama.** 2005. The N-terminal domain of thrombomodulin sequesters high-mobility group-B1 protein, a novel antiinflammatory mechanism. J. Clin. Investig. **115**:1267–1274.
2. **Agresti, A., and M. E. Bianchi.** 2003. HMGB proteins and gene expression. Curr. Opin. Genet. Dev. **13**:170–178.
3. **Albrecht, U., G. Eichele, J. A. Helms, and H. Lu.** 1997. Molecular and cellular methods in developmental toxicology. CRC Press, Boca Raton, FL.
4. **Andersson, U., H. Wang, K. Palmblad, A. C. Aveberger, O. Bloom, H. Erlandsson-Harris, A. Janson, R. Kokkola, M. Zhang, H. Yang, and K. J. Tracey.** 2000. High mobility group 1 protein (HMG-1) stimulates proinflammatory cytokine synthesis in human monocytes. J. Exp. Med. **192**:565–570.
5. **Ballock, R. T., and A. H. Reddi.** 1994. Thyroxine is the serum factor that regulates morphogenesis of columnar cartilage from isolated chondrocytes in chemically defined medium. J. Cell Biol. **126**:1311–1318.
6. **Binette, F., D. P. McQuaid, D. R. Haudenschild, P. C. Yaeger, J. M. McPherson, and R. Tubo.** 1998. Expression of a stable articular cartilage phenotype without evidence of hypertrophy by adult human articular chondrocytes in vitro. J. Orthop. Res. **16**:207–216.
7. **Blavier, L., and J. M. Delaisse.** 1995. Matrix metalloproteinases are obligatory for the migration of preosteoclasts to the developing marrow cavity of primitive long bones. J. Cell Sci. **108**(Pt. 12):3649–3659.
8. **Bonaldi, T., F. Talamo, P. Scaffidi, D. Ferrera, A. Porto, A. Bachi, A. Rubartelli, A. Agresti, and M. E. Bianchi.** 2003. Monocytic cells hyperacetylate chromatin protein HMGB1 to redirect it toward secretion. EMBO J. **22**: 5551–5560.
9. **Brett, J., A. M. Schmidt, S. D. Yan, Y. S. Zou, E. Weidman, D. Pinsky, R. Nowygrod, M. Neeper, C. Przysiecki, A. Shaw, et al.** 1993. Survey of the distribution of a newly characterized receptor for advanced glycation end products in tissues. Am. J. Pathol. **143**:1699–1712.
10. **Bustin, M.** 1999. Regulation of DNA-dependent activities by the functional motifs of the high-mobility-group chromosomal proteins. Mol. Cell. Biol. **19**:5237–5246.
11. **Calogero, S., F. Grassi, A. Aguzzi, T. Voigtlander, P. Ferrier, S. Ferrari, and M. E. Bianchi.** 1999. The lack of chromosomal protein Hmg1 does not disrupt cell growth but causes lethal hypoglycaemia in newborn mice. Nat. Genet. **22**:276–280.
12. **Charoonpatrapong, K., R. Shah, A. G. Robling, M. Alvarez, D. W. Clapp, S. Chen, R. P. Kopp, F. M. Pavalko, J. Yu, and J. P. Bidwell.** 2006. HMGB1 expression and release by bone cells. J. Cell Physiol. **207**:480–490.
13. **Degryse, B., T. Bonaldi, P. Scaffidi, S. Muller, M. Resnati, F. Sanvito, G. Arrigoni, and M. E. Bianchi.** 2001. The high mobility group (HMG) boxes of the nuclear protein HMG1 induce chemotaxis and cytoskeleton reorganization in rat smooth muscle cells. J. Cell Biol. **152**:1197–1206.
14. **Dumitriu, I. E., P. Baruah, B. Valentinis, R. E. Voll, M. Herrmann, P. P. Nawroth, B. Arnold, M. E. Bianchi, A. A. Manfredi, and P. Rovere-Querini.** 2005. Release of high mobility group box 1 by dendritic cells controls T-cell activation via the receptor for advanced glycation end products. J. Immunol. **174**:7506–7515.
15. **Engsig, M. T., Q. J. Chen, T. H. Vu, A. C. Pedersen, B. Therkidsen, L. R. Lund, K. Henriksen, T. Lenhard, N. T. Foged, Z. Werb, and J. M. Delaisse.** 2000. Matrix metalloproteinase 9 and vascular endothelial growth factor are essential for osteoclast recruitment into developing long bones. J. Cell Biol. **151**:879–889.
16. **Fukuyama, R., T. Fujita, Y. Azuma, A. Hirano, H. Nakamuta, M. Koida, and T. Komori.** 2004. Statins inhibit osteoblast migration by inhibiting Rac-Akt signaling. Biochem. Biophys. Res. Commun. **315**:636–642.
17. **Gerber, H. P., T. H. Vu, A. M. Ryan, J. Kowalski, Z. Werb, and N. Ferrara.** 1999. VEGF couples hypertrophic cartilage remodeling, ossification and angiogenesis during endochondral bone formation. Nat. Med. **5**:623–628.
18. **Gerstenfeld, L. C., S. D. Chipman, J. Glowacki, and J. B. Lian.** 1987. Expression of differentiated function by mineralizing cultures of chicken osteoblasts. Dev. Biol. **122**:49–60.
19. **Guazzi, S., A. Strangio, A. T. Franzi, and M. E. Bianchi.** 2003. HMGB1, an architectural chromatin protein and extracellular signalling factor, has a spatially and temporally restricted expression pattern in mouse brain. Gene Expr. Patterns **3**:29–33.
20. **Haaijman, A., R. N. D'Souza, A. L. Bronckers, S. W. Goei, and E. H. Burger.** 1997. OP-1 (BMP-7) affects mRNA expression of type I, II, X collagen, and matrix Gla protein in ossifying long bones in vitro. J. Bone Miner. Res. **12**:1815–1823.

Downloaded from mcb.asm.org by on April 3, 2008

21. **Hashimoto, S., R. L. Ochs, F. Rosen, J. Quach, G. McCabe, J. Solan, J. E. Seegmiller, R. Terkeltaub, and M. Lotz.** 1998. Chondrocyte-derived apoptotic bodies and calcification of articular cartilage. Proc. Natl. Acad. Sci. USA **95**:3094–3099.
22. **Henriksen, K., M. Karsdal, J. M. Delaisse, and M. T. Engsig.** 2003. RANKL and vascular endothelial growth factor (VEGF) induce osteoclast chemotaxis through an ERK1/2-dependent mechanism. J. Biol. Chem. **278**:48745–48753.
23. **Holmbeck, K., P. Bianco, J. Caterina, S. Yamada, M. Kromer, S. A. Kuznetsov, M. Mankani, P. G. Robey, A. R. Poole, I. Pidoux, J. M. Ward, and H. Birkedal-Hansen.** 1999. MT1-MMP-deficient mice develop dwarfism, osteopenia, arthritis, and connective tissue disease due to inadequate collagen turnover. Cell **99**:81–92.
24. **Imai, S., M. Kaksonen, E. Raulo, T. Kinnunen, C. Fages, X. Meng, M. Lakso, and H. Rauvala.** 1998. Osteoblast recruitment and bone formation enhanced by cell matrix-associated heparin-binding growth-associated molecule (HB-GAM). J. Cell Biol. **143**:1113–1128.
25. **Inada, M., Y. Wang, M. H. Byrne, M. U. Rahman, C. Miyaura, C. Lopez-Otin, and S. M. Krane.** 2004. Critical roles for collagenase-3 (Mmp13) in development of growth plate cartilage and in endochondral ossification. Proc. Natl. Acad. Sci. USA **101**:17192–17197.
26. **Kikuchi, T., T. Matsuguchi, N. Tsuboi, A. Mitani, S. Tanaka, M. Matsuoka, G. Yamamoto, T. Hishikawa, T. Noguchi, and Y. Yoshikai.** 2001. Gene expression of osteoclast differentiation factor is induced by lipopolysaccharide in mouse osteoblasts via Toll-like receptors. J. Immunol. **166**:3574–3579.
27. **Komori, T., H. Yagi, S. Nomura, A. Yamaguchi, K. Sasaki, K. Deguchi, Y. Shimizu, R. T. Bronson, Y. H. Gao, M. Inada, M. Sato, R. Okamoto, Y. Kitamura, S. Yoshiki, and T. Kishimoto.** 1997. Targeted disruption of Cbfa1 results in a complete lack of bone formation owing to maturational arrest of osteoblasts. Cell **89**:755–764.
28. **Lefebvre, V., S. Garofalo, G. Zhou, M. Metsaranta, E. Vuorio, and B. De Crombrugghe.** 1994. Characterization of primary cultures of chondrocytes from type II collagen/beta-galactosidase transgenic mice. Matrix Biol. **14**: 329–335.
29. **Lian, J. B., G. S. Stein, C. Stewart, E. Puchacz, S. Mackowiak, M. Aronow, M. Von Deck, and V. Shalhoub.** 1989. Osteocalcin: characterization and regulated expression of the rat gene. Connect. Tissue Res. **21**:61–69.
30. **Liu, W., S. Toyosawa, T. Furuichi, N. Kanatani, C. Yoshida, Y. Liu, M. Himeno, S. Narai, A. Yamaguchi, and T. Komori.** 2001. Overexpression of Cbfa1 in osteoblasts inhibits osteoblast maturation and causes osteopenia with multiple fractures. J. Cell Biol. **155**:157–166.
31. **McLeod, M. J.** 1980. Differential staining of cartilage and bone in whole mouse fetuses by alcian blue and alizarin red S. Teratology **22**:299–301.
32. **Mitola, S., M. Belleri, C. Urbinati, D. Coltrini, B. Sparatore, M. Pedrazzi, E. Melloni, and M. Presta.** 2006. Cutting edge: extracellular high mobility group box-1 protein is a proangiogenic cytokine. J. Immunol. **176**:12–15.
33. **Nakashima, K., and B. de Crombrugghe.** 2003. Transcriptional mechanisms in osteoblast differentiation and bone formation. Trends Genet. **19**:458–466.
34. **Nakashima, K., X. Zhou, G. Kunkel, Z. Zhang, J. M. Deng, R. R. Behringer, and B. de Crombrugghe.** 2002. The novel zinc finger-containing transcription factor osterix is required for osteoblast differentiation and bone formation. Cell **108**:17–29.
35. **Nomura, S., A. J. Wills, D. R. Edwards, J. K. Heath, and B. L. Hogan.** 1988. Developmental expression of 2ar (osteopontin) and SPARC (osteonectin) RNA as revealed by in situ hybridization. J. Cell Biol. **106**:441–450.
36. **Okubo, Y., and A. H. Reddi.** 2003. Thyroxine downregulates Sox9 and promotes chondrocyte hypertrophy. Biochem. Biophys. Res. Commun. **306**:186–190.
37. **Ortega, N., D. J. Behonick, and Z. Werb.** 2004. Matrix remodeling during endochondral ossification. Trends Cell Biol. **14**:86–93.
38. **Palumbo, R., M. Sampaolesi, F. De Marchis, R. Tonlorenzi, S. Colombetti, A. Mondino, G. Cossu, and M. E. Bianchi.** 2004. Extracellular HMGB1, a signal of tissue damage, induces mesoangioblast migration and proliferation. J. Cell Biol. **164**:441–449.
39. **Park, J. S., D. Svetkauskaite, Q. He, J. Y. Kim, D. Strassheim, A. Ishizaka, and E. Abraham.** 2004. Involvement of Toll-like receptors 2 and 4 in cellular activation by high mobility group box 1 protein. J. Biol. Chem. **279**:7370–7377.
40. **Park, K., B. H. Min, D. K. Han, and K. Hasty.** 2007. Quantitative analysis of temporal and spatial variations of chondrocyte behavior in engineered cartilage during long-term culture. Ann. Biomed. Eng. **35**:419–428.
41. **Passalacqua, M., M. Patrone, G. B. Picotti, M. Del Rio, B. Sparatore, E. Melloni, and S. Pontremoli.** 1998. Stimulated astrocytes release high-mobility group 1 protein, an inducer of LAN-5 neuroblastoma cell differentiation. Neuroscience **82**:1021–1028.
42. **Sakiyama, H., T. Nonaka, R. Masuda, N. Inoue, Y. Kuboki, M. Iijima, Y. Hirabayasi, M. Takahagi, K. Yoshida, K. Kuriiwa, M. Yoshida, and S. Imajoh-Ohmi.** 2002. Characterization of mineral deposits formed in cultures of a hamster tartrate-resistant acid phosphatase (TRAP) and alkaline phosphatase (ALP) double-positive cell line (CCP). Cell Tissue Res. **309**:269–279.
43. **Salmivirta, M., H. Rauvala, K. Elenius, and M. Jalkanen.** 1992. Neurite growth-promoting protein (amphoterin, p30) binds syndecan. Exp. Cell Res. **200**:444–451.
44. **Sato, T., M. del Carmen Ovejero, P. Hou, A. M. Heegaard, M. Kumegawa, N. T. Foged, and J. M. Delaisse.** 1997. Identification of the membrane-type matrix metalloproteinase MT1-MMP in osteoclasts. J. Cell Sci. **110**(Pt. 5): 589–596.
45. **Scaffidi, P., T. Misteli, and M. E. Bianchi.** 2002. Release of chromatin protein HMGB1 by necrotic cells triggers inflammation. Nature **418**:191–195.
46. **Schlueter, C., H. Weber, B. Meyer, P. Rogalla, K. Roser, S. Hauke, and J. Bullerdiek.** 2005. Angiogenetic signaling through hypoxia: HMGB1: an angiogenetic switch molecule. Am. J. Pathol. **166**:1259–1263.
47. **Stickens, D., D. J. Behonick, N. Ortega, B. Heyer, B. Hartenstein, Y. Yu, A. J. Fosang, M. Schorpp-Kistner, P. Angel, and Z. Werb.** 2004. Altered endochondral bone development in matrix metalloproteinase 13-deficient mice. Development **131**:5883–5895.
48. **Taguchi, A., D. C. Blood, G. del Toro, A. Canet, D. C. Lee, W. Qu, N. Tanji, Y. Lu, E. Lalla, C. Fu, M. A. Hofmann, T. Kislinger, M. Ingram, A. Lu, H. Tanaka, O. Hori, S. Ogawa, D. M. Stern, and A. M. Schmidt.** 2000. Blockade of RAGE-amphoterin signalling suppresses tumour growth and metastases. Nature **405**:354–360.
49. **Takami, M., N. Kim, J. Rho, and Y. Choi.** 2002. Stimulation by Toll-like receptors inhibits osteoclast differentiation. J. Immunol. **169**:1516–1523.
50. **Talreja, J., M. H. Kabir, B. F. M., D. J. Stechschulte, and K. N. Dileepan.** 2004. Histamine induces Toll-like receptor 2 and 4 expression in endothelial cells and enhances sensitivity to gram-positive and gram-negative bacterial cell wall components. Immunology **113**:224–233.
51. **Taniguchi, N., K. Kawahara, K. Yone, T. Hashiguchi, M. Yamakuchi, M. Goto, K. Inoue, S. Yamada, K. Ijiri, S. Matsunaga, T. Nakajima, S. Komiya, and I. Maruyama.** 2003. High mobility group box chromosomal protein 1 plays a role in the pathogenesis of rheumatoid arthritis as a novel cytokine. Arthritis Rheum. **48**:971–981.
52. **Vortkamp, A., K. Lee, B. Lanske, G. V. Segre, H. M. Kronenberg, and C. J. Tabin.** 1996. Regulation of rate of cartilage differentiation by Indian hedgehog and PTH-related protein. Science **273**:613–622.
53. **Vu, T. H., and Z. Werb.** 2000. Matrix metalloproteinases: effectors of development and normal physiology. Genes Dev. **14**:2123–2133.
54. **Wang, H., O. Bloom, M. Zhang, J. M. Vishnubhakat, M. Ombrellino, J. Che, A. Frazier, H. Yang, S. Ivanova, L. Borovikova, K. R. Manogue, E. Faist, E. Abraham, J. Andersson, U. Andersson, P. E. Molina, N. N. Abumrad, A. Sama, and K. J. Tracey.** 1999. HMG-1 as a late mediator of endotoxin lethality in mice. Science **285**:248–251.
55. **Wang, H., H. Yang, and K. J. Tracey.** 2004. Extracellular role of HMGB1 in inflammation and sepsis. J. Intern. Med. **255**:320–331.
56. **Wang, K., H. Yamamoto, J. R. Chin, Z. Werb, and T. H. Vu.** 2004. Epidermal growth factor receptor-deficient mice have delayed primary endochondral ossification because of defective osteoclast recruitment. J. Biol. Chem. **279**: 53848–53856.
57. **Yamada, S., K. Inoue, K. Yakabe, H. Imaizumi, and I. Maruyama.** 2003. High mobility group protein 1 (HMGB1) quantified by ELISA with a monoclonal antibody that does not cross-react with HMGB2. Clin. Chem. **49**: 1535–1537.
58. **Youn, J. H., and J. S. Shin.** 2006. Nucleocytoplasmic shuttling of HMGB1 is regulated by phosphorylation that redirects it toward secretion. J. Immunol. **177**:7889–7897.
59. **Zelzer, E., W. McLean, Y. S. Ng, N. Fukai, A. M. Reginato, S. Lovejoy, P. A. D'Amore, and B. R. Olsen.** 2002. Skeletal defects in VEGF(120/120) mice reveal multiple roles for VEGF in skeletogenesis. Development **129**:1893–1904.
60. **Zhou, Z., D. Immel, C. X. Xi, A. Bierhaus, X. Feng, L. Mei, P. Nawroth, D. M. Stern, and W. C. Xiong.** 2006. Regulation of osteoclast function and bone mass by RAGE. J. Exp. Med. **203**:1067–1080.

Downloaded from mcb.asm.org by on April 3, 2008

Intraocular Pressure Elevation after Injection of Triamcinolone Acetonide: A Multicenter Retrospective Case-Control Study

MASARU INATANI, KEIICHIRO IWAO, TAKAHIRO KAWAJI, YOSHIO HIRANO, YUICHIRO OGURA, KAZUYUKI HIROOKA, FUMIO SHIRAGA, YORIKO NAKANISHI, HIROYUKI YAMAMOTO, AKIRA NEGI, YUKA SHIMONAGANO, TAIJI SAKAMOTO, CHIEKO SHIMA, MIYO MATSUMURA, AND HIDENOBU TANIHARA

• PURPOSE: To determine the risk factors for intraocular pressure (IOP) elevation after the injection of triamcinolone acetonide (TA).

• DESIGN: Retrospective interventional case-control study.

• METHODS: SETTING: Multicenter. PATIENT POPULATION: Four hundred and twenty-seven patients. OBSERVATION PROCEDURES: Intraocular pressure levels after TA treatment by the sub-Tenon capsule injection (STI; 12 mg, 20 mg, or 40 mg), intravitreal injection (IVI; 4 mg or 8 mg), or the combination of STI (20 mg) and IVI (4 mg), and IOP levels after two TA treatments. MAIN OUTCOME MEASURE: Risk factors for IOP levels of 24 mm Hg or higher.

• RESULTS: Younger age (hazards ratio [HR], 0.96/year; $P < .0001$), IVI (HR, 1.89/year; $P < .0001$), and higher baseline IOP (HR, 1.15/mm Hg; $P = .003$) were identified as risk factors. Dose dependency was shown in STI-treated eyes (HR, 1.07/mg; $P = .0006$), as well as after IVI (HR, 1.64/mg; $P = .013$). The combination of STI and IVI was a significant risk factor (HR, 2.27; $P = .003$) compared with STI alone. In eyes receiving two TA treatments, IVI (HR, 2.60; $P = .010$), higher IOP elevation after the first injection (HR, 1.18/mm Hg; $P = .011$), and increased dosage of STI (HR, 1.07/mm Hg; $P = .033$) were risk factors.

• CONCLUSIONS: Younger age, higher baseline IOP, IVI, and increased TA dosage were associated with TA-induced IOP elevation. IOP elevation after repeated TA injection was frequently associated with eyes treated with IVI, high IOP elevation after the first injection, and high doses of STI. (Am J Ophthalmol 2008; 145:676–681. © 2008 by Elsevier Inc. All rights reserved.)

Accepted for publication Dec 6, 2007.

From the Department of Ophthalmology and Visual Science, Kumamoto University Graduate School of Medical Sciences, Kumamoto, Japan (M.I., K.I., T.K., H.T.); Department of Ophthalmology and Visual Science, Nagoya City University Graduate School of Medical Sciences, Nagoya, Japan (Y.H., Y.O.); Department of Ophthalmology, Kagawa University Faculty of Medicine, Miki, Japan (K.H., F.S.); Department of Organs Therapeutics, Division of Ophthalmology, Kobe University Graduate School of Medicine, Kobe, Japan (Y.N., H.Y., A.N.); Department of Ophthalmology, Faculty of Medicine, Kagoshima University Graduate School of Medicine and Dental Sciences, Kagoshima, Japan (Y.S., T.S.); and Department of Ophthalmology, Kansai Medical University, Moriguchi, Japan (C.S., M.M.).

Inquiries to Masaru Inatani, Department of Ophthalmology and Visual Science, Kumamoto University Graduate School of Medical Sciences, 1-1-1, Honjo, 860-8556 Kumamoto, Japan; e-mail: inatani@fc.kuh.kumamoto-u.ac.jp

TRIAMCINOLONE ACETONIDE (TA) IS COMMONLY USED to treat various vitreoretinal diseases. TA limits the impact of corticosteroids on ocular tissues, thereby minimizing the side effects associated with systemic steroid therapy.[1–5] However, many patients who have received intravitreal injection (IVI) of TA or the sub-Tenon capsule injection of TA (STI) encounter intraocular pressure (IOP) elevation,[6–13] which can develop into glaucoma.[14,15] The prevalence of TA-induced IOP elevation is reportedly between 18% and 50%.[7,13,16–19] This wide range of values might be explained by the following: variation between definitions of IOP elevation; the TA dose and the method of administration; whether patients have previously received TA injections; patient background characteristics, including history of glaucoma or ocular hypertension; and administration of steroids. Several reports have suggested an increased prevalence of TA-induced IOP elevation in younger patients.[1,7,15,20] Therefore, we retrospectively investigated the risk factors for IOP elevation in patients receiving TA at six Japanese clinical centers, based on a standardized definition of TA-induced IOP elevation.

METHODS

• PATIENTS: We reviewed the medical records of patients receiving TA by STI (12 mg, 20 mg, or 40 mg), IVI (4 mg or 8 mg), or simultaneous administration by STI (20 mg) and IVI (4 mg) at the following six clinical centers in Japan: Kumamoto University Hospital (Kumamoto), Nagoya City University Hospital (Nagoya), Kagawa University Hospital (Miki), Kobe University Hospital (Kobe), Kagoshima University Hospital (Kagoshima), and Kansai Medical University Hospital (Moriguchi). Data from patients who received TA between April 1, 2002 and March 31, 2006 were included in the analyses. If both eyes were treated with TA, the eye that was treated first was

© 2008 BY ELSEVIER INC. ALL RIGHTS RESERVED.

0002-9394/08/$34.00
doi:10.1016/j.ajo.2007.12.010

TABLE 1. Patient Data Before Triamcinolone Acetonide Treatment in < 24 mm Hg and ≥ 24 mm Hg Groups

Characteristic (n = 427)	Eyes with < 24 mm Hg (n = 377) n (%)	Eyes with ≥ 24 mm Hg (n = 50) n (%)	*p* value
Male gender	228 (60.5)	30 (60.0)	.948
Mean age (years)	65.8 ± 11.2	57.1 ± 17.5	.006*
Diabetes mellitus	203 (53.8)	17 (34.0)	.008*
Hypertension	137 (36.3)	18 (36.0)	.963
Cataract surgery	141 (37.4)	17 (34.0)	.638
Vitrectomy	88 (23.3)	14 (28.0)	.475
IVI included	69 (18.3)	25 (50.0)	<.0001*
Mean IOP at baseline (mm Hg)	13.8 ± 3.1	15.1 ± 3.1	.010*

IOP = intraocular pressure; IVI = intravitreal injection of triamcinolone acetonide.
*$P < .05$.

investigated. The exclusion criteria were as follows: eyes that had received intraocular surgery within three months before TA treatment; eyes with a history of glaucoma or uveitis; eyes that had shown > 21 mm Hg IOP levels; and patients who had been treated with steroids. Eyes treated with a second TA injection within the follow-up period were included in the analyses. If the TA dose administered in the second injection was different from that in the first, the eyes were included in the analysis of the first injection, but excluded from the analysis of the second.

• MAIN OUTCOME MEASURE AND OBSERVATION PROCEDURE: The main aim of this study was to investigate the risk factors for IOP elevation after TA treatment. The IOP levels after TA treatment were derived from patients' medical records. If any ocular surgeries were performed, IOP data from before the surgeries were evaluated. If an additional dose of TA was administered after the first injection, the IOP data at the first TA injection were evaluated until the second injection. The IOP levels were also evaluated between two weeks and a maximum of 12 months after the second injection. The baseline IOP was defined as the IOP level on the day of TA injection or at the last examination before the TA injection. The IOP data were mainly selected from records obtained by measurement using noncontact pneumotonometry. In line with previous reports,[6,15] we defined an IOP of 24 mm Hg or higher after TA treatment as elevated IOP induced by TA treatment. Furthermore, if IOP levels of 24 mm Hg or higher were shown by the noncontact pneumotonometer, they were re-examined using a Goldmann applanation tonometer on a slit-lamp biomicroscope, and the value shown by the tonometer was used as the IOP. Eyes for which the medical records did not indicate whether re-examination by tonometry had been performed were excluded from the study.

The following variables were assessed as potential risk factors for elevated IOP: gender; age; history of diabetes mellitus, hypertension, cataract surgery, or vitrectomy; dose and route of TA administration (12 mg, 20 mg, or 40 mg by STI; 4 mg or 8 mg by IVI; or a combination of 20 mg by STI and 4 mg by IVI); and baseline IOP. These factors were compared between patients with less than 24 mm Hg and those with 24 mm Hg or higher IOP. Potential risk factors for IOP levels of 24 mm Hg or higher after additional treatment were as described above. The maximal IOP minus baseline IOP (ΔIOP) values after the first treatment and the interval between the first and the second treatment were also assessed.

• STATISTICAL ANALYSIS: Data analysis was performed using the JMP version 6 statistical package program (SAS Institute, Cary, North Carolina, USA). The Mann–Whitney *U* test and the Chi-square test (or the Fisher exact test) were used for the univariate analyses. To confirm the effects of the risk factors and identify the hazard ratios (HRs) for TA-induced IOP elevation, multivariate Cox proportional hazards regression analysis was performed. The multivariate factors were selected from among the variants with a probability (*P*) value of less than .30 shown by univariate analysis. A *P* value less than .05 was considered statistically significant.

RESULTS

IN TOTAL, 427 EYES SATISFIED THE STUDY CRITERIA. ALL OF the eligible patients were Japanese. The diagnoses for the TA-treated eyes were as follows: age-related macular degeneration (67 eyes), other choroidal neovascular diseases (34 eyes), retinal vein occlusion (131 eyes), diabetic retinopathy (180 eyes), and other retinal diseases related to cystoid macular edema (15 eyes). Of these, 319 eyes were treated by one TA injection, and 108 eyes were treated with an additional TA injection. In total, 50 (11.7%) of the 427 eyes had an elevated IOP of 24 mm Hg or higher. IOP elevation of 24 mm Hg or above started 0.5

TABLE 2. Risk Factors for Elevated Intraocular Pressure Elevation of ≥ 24 mm Hg After Triamcinolone Acetonide Treatment—Cox Proportional Hazards Analysis

Variable	Hazards Ratio for ≥ 24 mm Hg	*p* value
Model 1: All eyes treated with triamcinolone acetonide injection (n = 427)		
Age (years)	0.96 (0.95 to 0.98)	<.0001*
Diabetes mellitus	0.76 (0.55 to 1.02)	.068
IVI included	1.89 (1.41 to 2.52)	<.0001*
IOP at baseline (mm Hg)	1.15 (1.05 to 1.27)	.003*
Model 2: Eyes with STI only (n = 333)		
Age (year)	0.96 (0.94 to 0.99)	.003*
Diabetes mellitus	0.91 (0.60 to 1.38)	.647
STI (mg)	1.07 (1.03 to 1.12)	.0006*
IOP at baseline (mm Hg)	1.31 (1.13–1.52)	.0003*
Model 3: Eyes with IVI only (n = 57)		
Age (year)	0.98 (0.94 to 1.03)	.393
Diabetes mellitus	0.91 (0.47 to 1.61)	.760
IVI (mg)	1.64 (1.09 to 3.39)	.013*
IOP at baseline (mm Hg)	1.03 (0.85 to 1.27)	.765
Model 4: Eyes with 20 mg of STI or 20 mg of STI plus 4 mg of IVI (n = 201)		
Age (year)	0.95 (0.92 to 0.98)	.003*
Diabetes mellitus	0.75 (0.41 to 1.29)	.306
Plus 4 mg of IVI	2.27 (1.33 to 4.02)	.003*
IOP at baseline (mm Hg)	1.28 (1.07 to 1.55)	.008*

IOP = intraocular pressure; IVI = intravitreal injection of triamcinolone acetonide; STI = sub-Tenon capsule injection of triamcinolone acetonide.
Hazards ratio is shown with 95% confidence interval.
*$P < .05$.

month after the injection in 12 eyes, after one month in nine eyes, after two months in 19 eyes, after three months in nine eyes, and after six months in one eye. Patient data before TA injection for the group with IOP elevation of less than 24 mm Hg and the group with 24 mm Hg or higher are shown in Table 1. The patients within the 24 mm Hg or higher group were younger, were less likely to have a history of diabetes mellitus, had a greater incidence of IVI administration of TA, and had higher baseline IOP values. The multivariate Cox proportional hazards regression showed that younger age (HR, 0.96 per year; 95% confidence interval [CI], 0.95 to 0.98; $P < .0001$), the inclusion of IVI (HR, 1.89; 95% CI, 1.41 to 2.52; $P < .0001$), and higher baseline IOP (HR, 1.15 per mm Hg; 95% CI, 1.05 to 1.27; $P = .003$) were risk factors for IOP elevation (Table 2; Model 1).

We also examined whether IOP elevation after TA injection was dose-dependent. In eyes treated by STI (n = 333), one of 36 eyes (2.8%), six of 164 eyes (3.7%), and 18 of 133 eyes (13.5%) showed IOP values of 24 mm Hg or higher after doses of 12 mg, 20 mg, and 40 mg by STI, respectively. Cox proportional hazards regression analysis of the 333 eyes identified younger age (HR, 0.96 per year; 95% CI, 0.94 to 0.99; $P = .003$), a higher dose administered by STI (HR, 1.07 per mg; 95% CI, 1.03 to 1.12; $P = .0006$), and higher baseline IOP (HR, 1.31 per mm Hg; 95% CI, 1.13 to 1.52; $P = .0003$) as risk factors (Table 2; Model 2). In eyes treated by IVI (n = 57), one of 18 eyes (5.6%) and 14 of 39 eyes (35.9%) were associated with IOP of 24 mm Hg or higher after doses of 4 mg and 8 mg by IVI, respectively. Cox proportional hazards regression analysis of the 57 eyes showed that a higher dose administered by IVI (HR, 1.64 per mg; 95% CI, 1.09 to 3.39; $P = .013$) was a risk factor. However, neither younger age (HR, 0.98 per year; 95% CI, 0.94 to 1.03; $P = .393$) nor higher baseline IOP (HR, 1.03 per mm Hg; 95% CI, 0.85 to 1.27; $P = .765$) were significant risk factors (Table 2; Model 3). Additionally, 10 of 37 eyes (27.0%) were associated with an IOP of 24 mm Hg or higher after simultaneous administration by STI (20 mg) and IVI (4 mg). In eyes treated with 20 mg by STI, or with both 20 mg by STI and 4 mg by IVI (n = 201), younger age (HR, 0.95 per year; 95% CI, 0.92 to 0.98; $P = .003$), the addition of 4 mg by IVI (HR, 2.27, 95% CI, 1.33 to 4.02; $P = .003$), and baseline IOP (HR, 1.28 per mm Hg; 95% CI, 1.07 to 1.55; $P = .008$) were identified as risk factors (Table 2; Model 4).

Of the 108 eyes treated with a second injection, 16 (14.8%) had IOP elevation to 24 mm Hg or higher. Data

TABLE 3. Data Before the Second Triamcinolone Acetonide Treatment in < 24 mm Hg and ≥ 24 mm Hg Groups

Characteristic (n = 108)	Eyes of < 24 mm Hg (n = 92) n (%)	Eyes of ≥ 24 mm Hg (n = 16) n (%)	p value
Male gender	53 (57.6)	10 (62.5)	.714
Mean age (years)	63.1 ± 11.0	55.6 ± 17.8	.279
Diabetes mellitus	50 (54.3)	8 (50.0)	.748
Hypertension	42 (45.7)	3 (18.8)	.044*
Cataract surgery	33 (35.9)	6 (37.5)	.900
Vitrectomy	24 (26.1)	5 (31.3)	.667
IVI included	4 (4.3)	4 (25.0)	.004*
Mean IOP at baseline (mm Hg)	13.8 ± 3.0	13.5 ± 2.4	.900
ΔIOP after the 1st injection (mm Hg)	3.0 ± 3.2	5.8 ± 2.1	<.0001*
Interval between 1st and 2nd injections (months)	5.2 ± 3.2	5.1 ± 3.2	.841

IOP = intraocular pressure; IVI = intravitreal injection of triamcinolone acetonide; ΔIOP = maximal IOP minus baseline IOP.
*$P < .05$.

TABLE 4. Risk Factors for Elevated Intraocular Pressure of ≥ 24 mm Hg After Second Triamcinolone Acetonide Injection—Cox Proportional Hazards Analysis

Variable (n = 108)	Hazards ratio for ≥ 24 mm Hg	p value
Model 1: All the eyes treated with repeated TA injections (n = 108)		
Age (years)	0.99 (0.95 to 1.02)	.410
Hypertension	0.71 (0.33 to 1.29)	.276
IVI included	2.60 (1.30 to 4.83)	.010*
ΔIOP after 1st injection (mm Hg)	1.18 (1.04 to 1.30)	.011*
Model 2: Eyes with repeated STIs (n = 100)		
Age (years)	1.03 (0.98 to 1.08)	.247
Hypertension	0.82 (0.37 to 1.58)	.557
STI (mg)	1.07 (1.01 to 1.18)	.033*
ΔIOP after 1st injection (mm Hg)	1.45 (1.17 to 1.85)	.0006*

IVI = intravitreal injection of triamcinolone acetonide; STI = sub-Tenon capsule injection of triamcinolone acetonide; ΔIOP = maximal IOP minus baseline IOP.
Hazards ratio is shown with 95% confidence interval.
*$P < .05$.

before the second TA treatment for the group with elevation of less than 24 mm Hg and the group with elevation of 24 mm Hg or higher are shown in Table 3. The 24 mm Hg or higher group included fewer patients with histories of hypertension, more eyes treated with the inclusion of IVI, and higher ΔIOP after the first injection. Cox proportional hazards regression analysis showed that the inclusion of IVI (HR, 2.60; 95% CI, 1.30 to 4.83; $P = .010$) and higher ΔIOP after the first injection (HR,1.18 per mm Hg; 95% CI, 1.04 to 1.30; $P = .011$) were risk factors for IOP elevation after the additional TA injection (Table 4; Model 1). In eyes treated with two STI injections (n = 100), an increased dose administered by STI (HR, 1.07 per mg; 95% CI, 1.01 to 1.18; $P = .033$) and higher ΔIOP after the first injection (HR, 1.45 per mm Hg; 95% CI, 1.17 to 1.85; $P = .0006$) were shown to be risk factors (Table 4; Model 2).

DISCUSSION

THIS STUDY INVESTIGATED THE RISK FACTORS OF IOP ELEvation following topical TA injection. Cox proportional hazards regression analysis of 427 eyes showed that younger age (HR, 0.96 per year; 95% CI, 0.95 to 0.98), TA treatment including IVI (HR, 1.89; 95% CI, 1.41 to 2.52), and higher baseline IOP (HR, 1.15 per year; 95% CI;1.05 to 1.27) were risk factors for elevated IOP of 24 mm Hg or

higher. These risk factors were also observed in the 201 eyes treated with either 20 mg by STI or a combination of 20 mg by STI and 4 mg by IVI. TA dose dependency for the frequency of IOP elevation was identified by multivariate analyses for 333 eyes treated by STI (1.07 per mg; 95% CI, 1.03 to 1.12) and 57 eyes treated by IVI (1.64 per mg; 95% CI, 1.09 to 3.39). Moreover, multivariate analyses in eyes after two TA treatments showed that TA treatment including IVI, higher ΔIOP after the first TA injection, and a higher dose administered by STI were risk factors.

Several reports have discussed the rates of IOP elevation after TA injection, and have identified potential risk factors. Retrospective studies examining IVI-induced IOP elevation reported that treatment with 20 mg by IVI induced IOP of more than 21 mm Hg in 112 of 272 patients (41.2%),[1] and that 4 mg by IVI induced IOP elevation by 30% or more in 267 of 528 eyes (50.6%),[12] IOP elevation to 24 mm Hg or higher in 36 of 89 patients (40.4%),[6] and IOP elevation to more than 21 mm Hg, or by more than 5 mm Hg, in 26 of 60 patients (43.3%).[20] These results indicate that higher baseline IOP values[6,12] and younger age[1,20] are risk factors for IVI-induced IOP elevation.

By contrast, retrospective studies of STI-induced IOP elevation showed levels equal to or more than 6 mm Hg, or IOP levels of more than 20 mm Hg, in nine of 49 eyes (18.4%),[13] and IOP elevation of equal to or more than 5 mm Hg in 19 of 43 eyes (44.2%).[8] In our previous retrospective study, 40 mg by STI induced high IOP of 24 mm Hg or above in 26 of 115 eyes (22.6%).[15] Younger age[15] and a history of diabetes mellitus[13] are reported risk factors for STI-induced IOP elevation. However, to determine in detail the influence of risk factors, including the dose and route of TA administration, it will be necessary to carry out statistical analysis on a larger number of eyes treated with TA at multiple clinical centers. In this meta-study, to determine the TA-induced IOP elevation more exactly, we excluded eyes with other risk factors for IOP elevation, such as glaucoma, ocular hypertension, uveitis, steroid administration, and recent histories of intraocular surgery. Moreover, TA-induced IOP elevation obtained using noncontact pneumotonometry was confirmed using a Goldmann applanation tonometer. Taken together, our retrospective results reflect the detailed characterization of TA-induced IOP elevation.

No previous large-scale clinical studies have confirmed the risk factors for TA-induced IOP, or examined the effects of the amount of TA administered and the interaction between STI and IVI. The present study not only confirmed that younger age and higher baseline IOP risk factors,[1,6,12,20] but also revealed that IVI induces IOP elevation more frequently than STI, as well as demonstrating the dose dependency for TA-induced IOP elevation. However, no correlations with gender, medical history of hypertension, diabetes mellitus, cataract surgery, or vitrectomy were observed in the analyses for the risk factors. Although some reports have shown that diabetes mellitus is a risk factor for corticosteroid-induced IOP elevation,[13,21] others have shown that it is not significant. A previous randomized diabetes mellitus clinical trial conducted by Palmberg[22] showed that the history of diabetes mellitus was not associated with glaucoma. Our results seem to agree with this. In addition, it could be speculated that the lens and the vitreous affect the diffusion of TA in the ocular tissue; however, no reports (including our present results) suggest that the histories of cataract surgery and vitreous surgery influence TA-induced ocular hypertension.

Interestingly, IVI and ΔIOP are risk factors for IOP elevation in eyes treated with repeated TA injections. IOP elevation is also frequently associated with a higher dose of repeated STI treatment. There are some reports concerning IOP elevation after repeated TA injection.[6,7,12] A study that retrospectively investigated 43 eyes treated repeatedly with 20 to 25 mg by IVI showed that no eyes with 21 mm Hg or less after the first TA injection exhibited more than 21 mm Hg after the second TA injection.[24] By contrast, another study previously reported that 28 of 43 eyes (65.1%) treated with a second TA injection showed an IOP elevation of 30% or more, which was not observed at the first TA injection.[12] In our present study, 15 of 16 eyes with IOP elevation after the second TA injection did not exhibit IOP elevation after the first TA injection. Our present data appear to agree with the latter study, although it showed that the risk factors for IOP elevation after the second TA injection were higher baseline IOP and male gender.[12]

The study presented here has several limitations. First, it shows the risk factors for IOP elevation and not for TA-induced visual field loss attributable to severe TA-induced ocular hypertension. We could not retrospectively quantify visual field loss in eyes with TA-induced IOP elevation because of the association with retinal macular diseases. Second, we did not statistically analyze the duration of IOP elevation in this study. In total, 44 of 50 eyes with IOP elevation in this study showed reversible IOP elevation, whereas six eyes were associated with persistent ocular hypertension in spite of anti-glaucomatous medical treatments. They were treated with trabeculectomy (two eyes) and trabeculotomy (four eyes), which is a surgical procedure effective for corticosteroid-induced glaucoma.[15,23] The six eyes included three treated with 8 mg by IVI, one treated with 4 mg by IVI, one treated with 4 mg by IVI plus 20 mg by STI, and one treated with 40 mg by STI. Persistent IOP elevation might be associated with IVI or high-dose treatment by STI. Third, it remains to be determined whether glaucoma and ocular hypertension are risk factors, as we excluded patients suffering from these disorders from the present study. Such patients might be more

susceptible to TA-induced IOP elevation. Actually, few cases with past histories of glaucoma and ocular hypertension were treated with TA injection. In our clinical centers, TA injection might have been avoided in the patients associated with glaucoma or ocular hypertension. Fourth, we could not evaluate worldwide differences as we only analyzed data from Japanese patients.

In conclusion, our case-control study indicates that younger patients, those with a higher baseline IOP, and those receiving higher doses of TA or intravitreally administered TA are more susceptible to corticosteroid-induced IOP elevation. Greater IOP elevation after the first injection is associated with frequent IOP elevations after the second TA injection.

THIS STUDY WAS SUPPORTED IN PART BY GRANTS-IN-AID FOR SCIENTIFIC RESEARCH FROM THE MINISTRY OF EDUCATION, Science, Sports, and Culture, Japan, and from the Ministry of Health and Welfare, Tokyo, Japan. The authors indicate no financial conflict of interest. Involved in design and conduct of study (M.I., K.I., H.T.); collection and management of the data (K.I., T.K., Y.H., Y.O., K.H., F.S., Y.N., H.Y., A.N., Y.S., T.S., C.S., M.M.); analysis (M.I., K.I.); interpretation of the data (M.I.); preparation of the first draft manuscript (M.I.), and in reviewing and approval of the manuscript (Y.O., F.S., A.N., T.S., M.M., H.T.). All procedures conformed to the Declaration of Helsinki and informed consent was obtained from each of the patients participating in the study. The retrospective interventional case-control study was approved by the Institutional Review Board of Kumamoto University Hospital (Kumamoto, Japan).

REFERENCES

1. Jonas JB, Kreissig I, Degenring R. Intravitreal triamcinolone acetonide for treatment of intraocular proliferative, exudative, and neovascular diseases. Prog Retin Eye Res 2005;24: 587–611.
2. Kawaji T, Hirata A, Awai N, et al. Trans-tenon retrobulbar triamcinolone injection for macular edema associated with branch retinal vein occlusion remaining after vitrectomy. Am J Ophthalmol 2005;140:540–542.
3. Antcliff RJ, Spalton DJ, Stanford MR, Graham EM, Ffytche TJ, Marshall J. Intravitreal triamcinolone for uveitic cystoid macular edema: an optical coherence tomography study. Ophthalmology 2001;108:765–772.
4. Danis RP, Ciulla TA, Pratt LM, Anliker W. Intravitreal triamcinolone acetonide in exudative age-related macular degeneration. Retina 2000;20:244–250.
5. Greenberg PB, Martidis A, Rogers AH, Duker JS, Reichel E. Intravitreal triamcinolone acetonide for macular edema due to central retinal vein occlusion. Br J Ophthalmol 2002;86: 247–248.
6. Smithen LM, Ober MD, Maranan L, Spaide RF. Intravitreal triamcinolone acetonide and intraocular pressure. Am J Ophthalmol 2004;138:740–743.
7. Jonas JB, Kreissig I, Degenring R. Intraocular pressure after intravitreal injection of triamcinolone acetonide. Br J Ophthalmol 2003;87:24–27.
8. Jea SY, Byon IS, Oum BS. Triamcinolone-induced intraocular pressure elevation: intravitreal injection for macular edema and posterior subtenon injection for uveitis. Korean J Ophthalmol 2006;20:99–103.
9. Benz MS, Albini TA, Holz ER, et al. Short-term course of intraocular pressure after intravitreal injection of triamcinolone acetonide. Ophthalmology 2006;113:1174–1178.
10. Ozkiris A, Erkilic K. Complications of intravitreal injection of triamcinolone acetonide. Can J Ophthalmol 2005;40:63–68.
11. Yamashita T, Uemura A, Kita H, Sakamoto T. Intraocular pressure after intravitreal injection of triamcinolone acetonide following vitrectomy for macular edema. J Glaucoma 2007;16:220–224.
12. Rhee DJ, Peck RE, Belmont J, et al. Intraocular pressure alterations following intravitreal triamcinolone acetonide. Br J Ophthalmol 2006;90:999–1003.
13. Hirooka K, Shiraga F, Tanaka S, Baba T, Mandai H. Risk factors for elevated intraocular pressure after trans-tenon retrobulbar injections of triamcinolone. Jpn J Ophthalmol 2006;50:235–238.
14. Kaushik S, Gupta V, Gupta A, Dogra MR, Singh R. Intractable glaucoma following intravitreal triamcinolone in central retinal vein occlusion. Am J Ophthalmol 2004;137: 758–760.
15. Iwao K, Inatani M, Kawaji T, Koga T, Mawatari Y, Tanihara H. Frequency and risk factors for intraocular pressure elevation after posterior sub-Tenon capsule triamcinolone acetonide injection. J Glaucoma 2007;16:251–256.
16. Bakri SJ, Beer PM. The effect of intravitreal triamcinolone acetonide on intraocular pressure. Ophthalmic Surg Lasers Imaging 2003;34:386–390.
17. Gillies MC, Simpson JM, Billson FA, et al. Safety of an intravitreal injection of triamcinolone: results from a randomized clinical trial. Arch Ophthalmol 2004;122: 336–340.
18. Park CH, Jaffe GJ, Fekrat S. Intravitreal triamcinolone acetonide in eyes with cystoid macular edema associated with central retinal vein occlusion. Am J Ophthalmol 2003;136: 419–425.
19. Massin P, Audren F, Haouchine B, et al. Intravitreal triamcinolone acetonide for diabetic diffuse macular edema: preliminary results of a prospective controlled trial. Ophthalmology 2004; 111:218–224.
20. Park HY, Yi K, Kim HK. Intraocular pressure elevation after intravitreal triamcinolone acetonide injection. Korean J Ophthalmol 2005;19:122–127.
21. Becker B, Bresnick G, Chevrette L, Kolker AE, Oaks MC, Cibis A. Intraocular pressure and its response to topical corticosteroids in diabetes. Arch Ophthalmol 1966;76:477–483.
22. Palmberg P. Screening for diabetic retinopathy. Diabetes Care 2001;24:419–420.
23. Honjo M, Tanihara H, Inatani M, Honda Y. External trabeculotomy for the treatment of steroid-induced glaucoma. J Glaucoma 2000;9:483–485.
24. Jonas JB, Degenring R, Kreissig I, Akkoyun I. Safety of intravitreal high-dose reinjections of triamcinolone acetonide. Am J Ophthalmol 2004;138:1054–1055.

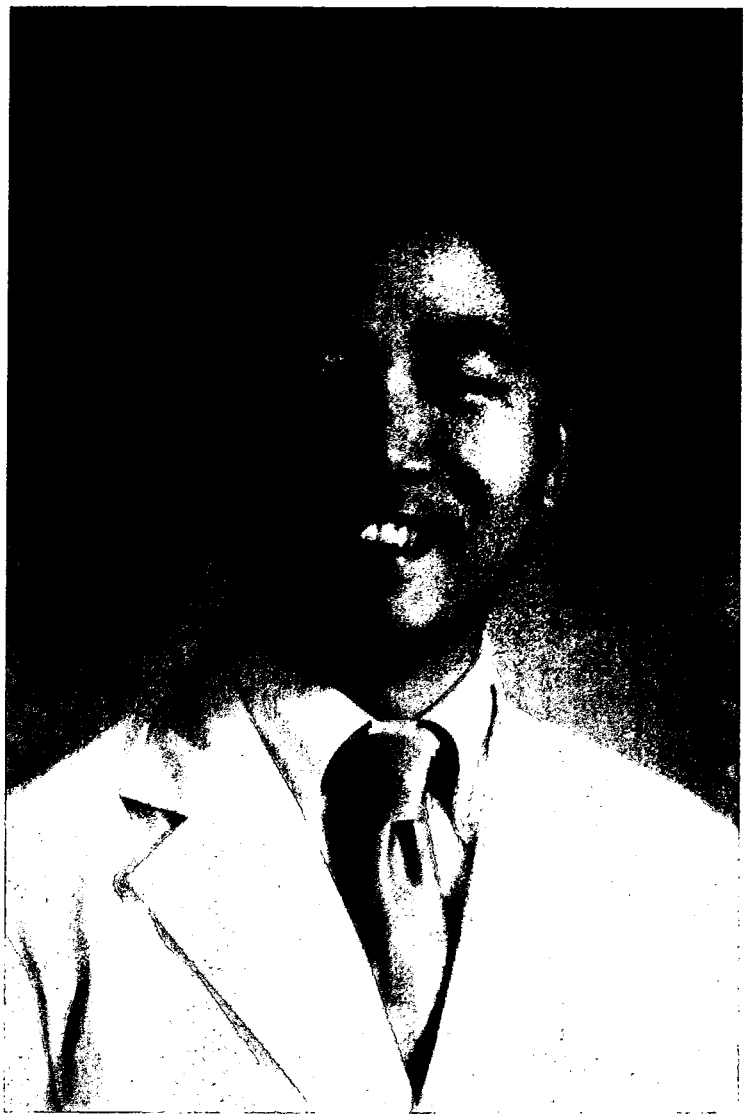

Biosketch

Masaru Inatani, MD, PhD, received his doctorate, which was on optic nerve guidance, from Kyoto University's Graduate School of Medicine in 2005. Dr Inatani is presently an Associate Professor at Department of Ophthalmology, Kumamoto University Hospital, Kumamoto, Japan. His interests include glaucoma surgery and the mechanisms of glaucoma optic neuropathy.

[Cancer Biology & Therapy 6:8, 1276-1283; August 2007]; ©2007 Landes Bioscience

Research Paper

Inhibition of Melanoma by Ultrasound-Microbubble-Aided Drug Delivery Suggests Membrane Permeabilization

Shozo Sonoda[1]
Katsuro Tachibana[2]
Eisuke Uchino[1]
Toshifumi Yamashita[1]
Kenji Sakoda[3]
Koh-Hei Sonoda[4]
Toshio Hisatomi[4]
Yuichi Izumi[3]
Taiji Sakamoto[1,*]

[1]Department of Ophthalmology; [3]Department of Periodontology; Graduate School of Medical and Dental Sciences; Kagoshima University; Kagoshima, Japan

[2]Department of Anatomy; Fukuoka University School of Medicine; Fukuoka, Japan

[4]Department of Ophthalmology; Graduate School of Medical Sciences; Kyushu University; Fukuoka, Japan

*Correspondence to: Taiji Sakamoto; Department of Ophthalmology; Graduate School of Medical and Dental Sciences; Kagoshima University; 8-35-1 Sakuragaoka; Kagoshima 890-8520 Japan; Tel.: +81.99.275.5402; Fax: +81.99.265.4894; Email: tsakamot@m3.kufm.kagoshima-u.ac.jp

Original manuscript submitted: 03/22/07
Revised manuscript submitted: 05/23/07
Manuscript accepted: 05/24/07

Previously published as a *Cancer Biology & Therapy* E-publication:
http://www.landesbioscience.com/journals/cbt/article/4485

KEY WORDS

ultrasound, drug delivery, microbubbles, anti-tumor effect, melanoma, sonoporation, bleomycin

ACKNOWLEDGEMENTS

This work was supported by Grants-in-Aid for Scientific Research from Ministry of Education, Science and Culture of Japanese Government (17659550 and 18791287).

ABSTRACT

Ultrasound exposure-induced cavitation has been shown to accentuate cell membrane permeability, thus promoting effective drug delivery into cells, a technique that can be enhanced in the presence of microbubbles (MB). Here we applied this method as a treatment for malignant melanoma of the eyelid. The incidence of malignant melanoma in ophthalmology is relatively high, but its treatment is cosmetically difficult. A greater in vitro growth suppression of B-16 melanoma cells was achieved using ultrasound and MB in combination with the anticancer drug bleomycin than when a more concentrated dose of bleomycin alone was applied to the cell culture. Moreover, this effect was enhanced in an in vivo tumor model created by injecting B-16 melanoma cells into the lower eyelids of SCID mice. The antitumor effect of bleomycin was observed at a lower dose (0.5 mg/ml) when the treatment was used in conjunction with ultrasound. The effect was further enhanced when MB were included, with tumor shrinkage occurring at bleomycin levels of 0.06 mg/ml. These results show that ultrasound and MB promote efficient bleomycin uptake by cells, and that the technique is a potentially useful drug delivery method.

INTRODUCTION

In the field of melanoma oncology there continues to be a series of patients that have cancers resistant to standard chemotherapeutic agents. Certainly in other malignancies new chemotherapeutic approaches have demonstrated significant benefit.[1,2] This is less to do with drug efficacy than with the difficulties involved in achieving specific delivery to a target organ while minimizing adverse effects on surrounding healthy tissue.

Ultrasonic therapy has been used for some time in the treatment of cancer.[3-9] In the early stages of its development, attempts were made to destroy cancer cells by using high energy to raise the temperature of the target organ.[10-12] However, this method adversely affected healthy tissue, meaning that its benefits were limited. It has recently been reported that low-energy ultrasound that does not raise tissue temperature, dramatically increases the effectiveness of anticancer agents.[13-16] The mechanism behind this anticancer effect of ultrasound is not well understood, but one possibility is that it causes sonoporation: the development of small pores in the cell membrane caused by the effects of cavitation.[8,17] This low-energy ultrasound method has been used in previous attempts to introduce drugs and genes into cells, but the establishment of the necessary conditions has proved technically difficult.[18,19] If the ultrasound is too weak, transduction efficiency will be low, whereas higher-temperature ultrasound risks damaging healthy cells. For this reason, the method has not reached the stage of clinical application. However, should the resolution of these technical difficulties make its application possible, ultrasound would enable the selective application of drug therapy to target organs with minimal adverse reactions.

Microbubbles (MB), fine bubbles approximately 2-μm in diameter, are used clinically as an ultrasonic contrast medium.[20-22] MB have a unique resonant frequency and, when ultrasound is exposed at that frequency, the MB resonate easily and burst. When ultrasound is irradiated onto a solution containing MB, cavitation will occur, even at frequencies low enough to preclude the risk of damaging cells.[23,24] In this way, it is theoretically possible to deliver substances such as anticancer drugs using ultrasound in a manner that is not harmful to cells.[25-27]

In the present study, we investigated the application of ultrasound of MB as a treatment for malignant melanoma of the eyelid. Melanomas of the eye can involve various ocular structures including the eyelid conjunctiva and uvea, but its treatment is difficult. The reduction of tumor size with this method would therefore be of clinical significance.

MATERIALS AND METHODS

Cell culture. Mouse B-16 melanoma cells (5 x 10^6; ATCC, Manassas, VA) were cultured in modified Eagles's medium (MEM. Sigma-Aldrich, St. Louis, MO) with 10% fetal bovine serum (FBS. Invitrogen-Gibco, Grand Island, NY) and streptomycin/penicillin (Wako, Osaka, Japan) at 37°C under 5% CO_2. Cells were subcultured at 80% confluency and used between passages P4–P6.

Ultrasound. Ultrasonic conditions were optimized to prevent cell damage. B-16 cells (3.2 x 10^4) were seeded in each well of a 24-well dish with 1 ml MEM supplemented with 10% FBS. A 6-mm diameter Sonitron 2000^{TM} probe (Rich Mar Inc., Inola, OK) was used for ultrasonic irradiation. The probe was inserted directly into the wells of the dish and secured 3 mm above the bottom. Ultrasound irradiation was performed at 1MHz frequency using the following conditions: 1 W/cm^2 power density, 10% duty cycle, 60 s duration; 1 W/cm^2 power density, 50% duty cycle, 60 s duration; 1 W/cm^2 power density, 100% duty cycle, 60 s duration; 1 W/cm^2 power density, 10% duty cycle, 120 s duration; 1 W/cm^2 power density, 50% duty cycle, 120 s duration; 1 W/cm^2 power density, 100% duty cycle, 120 s duration; 2 W/cm^2 power density, 10% duty cycle, 60 s duration; 2 W/cm^2 power density, 50% duty cycle, 60 s duration; 2 W/cm^2 power density, 100% duty cycle, 60 s duration; 2 W/cm^2 power density, 10% duty cycle, 120 s duration; 2 W/cm^2 power density, 50% duty cycle, 120 s duration; 2 W/cm^2 power density, 100% duty cycle, 120 s duration. Cell counts were taken 24, 48, 72 and 96 h after irradiation and the cell growth curve compared with a control group that was not ultrasonically irradiated.

Microbubbles. Cells were diluted to 3.2 x 10^4 cells per 100 µl medium. Optison ^{TM} microbubbles (10, 20 or 40 µl; MB; Amersham Health, Princeton, NJ) were added to each sample and mixed for 5 min. Each sample was transferred to one well of a 48-well dish, which was filled up to 500 µl with MEM medium containing 10% FBS. Cell counts were taken 24, 48, 72 and 96 h after the start of culturing and a cell growth curve was plotted. Using the method described above, an Optison mixture was prepared and irradiated at 1 W/cm^2 power density, 50% duty cycle, and 60 s duration, followed by 2 W/cm^2 power density, 50% duty cycle and 60 s duration. Damage to cells when the MB and ultrasound were used in combination was studied using cell counts and growth curve comparisons as described above. Cells were assessed 24, 48, 72 and 96 h after irradiation.

Effects of bleomycin according to dose method. Bleomycin only. Cells were adjusted to 3.2 x 10^4 cells per well of a 24-well dish. Bleomycin (Nippon Kayaku, Tokyo, Japan) was dissolved in MEM media and adjusted to 5, 0.5, 0.05, 0.005, 0.0005 and 0.00005 µM. Each solution (1 ml) was added to each well. Cell counts were taken 24, 48, 72 and 96 h after the start of culturing and a cell growth curve was plotted. After 24 h, the culture medium was replaced with MEM containing 10% FBS. Experiments were repeated at least three times.

Ultrasound and bleomycin. Six cell/bleomycin mixtures were prepared as above. Ultrasonic irradiation was carried out at 1 W/cm^2 power density, 50% duty cycle and 60 s duration. These conditions did not cause any damage to cells. Cell counts were taken 24, 48, 72 and 96 h after irradiation.

Ultrasound and MB and bleomycin. Six cell/bleomycin mixtures were prepared with 3.2 x 10^4 cells per 100 µl. Optison (5, 10 or 20 µl) was added to one tube of each sample and stirred for 5 min. Each sample was then transferred to one well of a 24-well dish and culture medium added to a total of 1 ml. Ultrasonic irradiation was performed at 1 W/cm^2 power density, 50% duty cycle and 60 s duration. Cell counts were taken as described above.

Calculation of cell count. Cells were counted from digital photographs (IX71, Olympus, Tokyo, Japan) at three random sites per well using NIH Image analysis software (Bethesda, MD) by an examiner who was blind to the experimental details. The mean value for two subjects was regarded as the cell count for each condition. The cell counts were plotted and a cell growth curve drawn. At least three experiments were performed for each condition.

Animals. Five-week-old male SCID mice (n = 5) were anesthetized with an intraperitoneal injection of a mixed solution of ketamine hydrochloride (Ketalal, 60 mg/kg) and medetomidine (Domital, 0.3 mg/kg). After obtaining the approval of the Kagoshima University board, all animal experiments were conducted humanely in strict compliance with the ARVO statement for the Use of Animals in Ophthalmic and Vision Research.

P4-5 B-16 cells were harvested and diluted in PBS to a concentration of 1 x 10^6 cells per 50 µl. Under anaesthetic, a 2 x 2-cm area of hair extending from the lower left eyelid to the periphery of the auricle was shaved. Next, 1 x 10^6 cells were injected with a 30G needle using a magnifying glass. Observations were made every two days after the injection, and the experiment commenced when the diameter of the largest tumor reached 4–5 mm.

Bleomycin was injected into the center of tumor using a syringe with a 30 G needle. Immediately thereafter, a 6-mm US probe was placed directly on the tumor surface and US was generated. Every two days after the start of each experiment, each animal's weight and the diameters of the smallest and largest tumors were measured. The estimated tumor weight and mean relative tumor weight were calculated based on the following formulas[28]: Estimated tumor weight = largest diameter (mm) x smallest diameter (mm)^2 x 0.5. Mean relative tumor weight = estimated tumor weight at each measurement point / estimated tumor weight at the start of administration.

The bleomycin anti-tumor effect was evaluated as the index of the mean relative tumor weight.

Evaluation of bleomycin anti-tumor effect. Bleomycin was dissolved in PBS to a concentration of 2 mg/ml and two-fold serial dilution of 1, 0.5, 0.25, 0.125 and 0.06 mg/ml were prepared.

Mice (n = 5–7) were injected with 50 µl bleomycin at 2, 1, 0.5 and 0.25 mg/ml on days 0, 2, 4 and 6. The tumor size and weight were measured two times before injection on days 0–6 and every second day after completion of the injections.

Next, the anti-tumor effects of delivering bleomycin in combination with ultrasound were investigated. Ultrasonic irradiation was performed at 2 W/cm^2 power density, 50% duty cycle, and 240 s duration. These conditions had been shown in previous experiments to cause virtually no tissue damage.[23] Mouse tumors were injected with 50 µl bleomycin at 1, 0.5, 0.25, 0.125 and 0.06 mg/ml prior to ultrasonic irradiation directed onto the tumor site using the 6 mm Sonitron 2000^{TM} probe. The number of injections and tumor size were calculated as described above.

Next, the anti-tumor effects of bleomycin, administered in combination with both ultrasound, and MB were investigated. Ten microliters MB was added to 50 µl bleomycin at 0.5, 0.25, 0.125 and 0.06 mg/ml, and each solution was mixed slowly for 1 min. The mixtures were injected into the tumor, which was then ultrasonically irradiated at 2 W/cm^2 power density, 50% duty cycle, and 240 s duration. Injections and measurements were performed as described earlier.

Table 1 **Optimal conditions of ultrasound irradiation for B-16**

Power	Duty Cycle	Duration	24 h	48 h	72 h	96 h
1 W/cm^2	10%	60 sec	425.00 ± 38.19	516.67 ± 72.65	565.00 ± 21.79	783.33 ± 65.09
		120 sec	360.00 ± 44.44	400.00 ± 57.74	550.00 ± 104.08	866.67 ± 72.65
2 W/cm^2		60 sec	373.33 ± 14.53	466.67 ± 33.33	616.67 ± 60.09	916.67 ± 60.09
		120 sec	466.67 ± 72.65	575.00 ± 43.30	700.00 ± 50.00	816.67 ± 72.65
1 W/cm^2	50%	60 sec	541.25 ± 49.48	831.25 ± 54.36	2005.00 ± 407.57	5225.00 ± 257.91
		120 sec	520.00 ± 34.94	781.25 ± 62.40	1425.00 ± 283.95	4750.00 ± 542.76
2 W/cm^2		60 sec	492.86 ± 49.75	795.71 ± 45.71	1500.00 ± 283.68	4507.14 ± 469.10
		120 sec	493.33 ± 103.49	783.33 ± 94.05	1366.67 ± 72.65	4383.33 ± 60.09
1 W/cm^2	100%	60 sec	75.00 ± 14.43	100.00 ± 0.00	91.67 ± 8.33	116.67 ± 30.05
		120 sec	100.00 ± 14.43	83.33 ± 16.67	83.33 ± 16.67	83.33 ± 16.67
2 W/cm^2		60 sec	83.33 ± 16.67	75.00 ± 14.43	75.00 ± 14.43	83.33 ± 16.67
		120 sec	56.67 ± 9.28	58.33 ± 8.33	58.33 ± 8.33	58.33 ± 8.33
	control		605.75 ± 77.43	863.50 ± 85.34	2460.00 ± 380.08	5906.25 ± 211.38

mean ± S.E.

As a control for the three experiments described above, SCID mice were injected with 50 µl PBS and weight and tumor size measured every two days from the start of the experiment.

Evaluation of ultrasound/optison anti-tumor effects. To evaluate the effects of ultrasound alone on the efficacy of drug delivery, 50 µl PBS was injected into each tumor, which was then ultrasonically irradiated four times at 2 W/cm^2 power density, 50% duty cycle, and 240 s duration. The size of the tumor was measured two times before the injection and every second day after the completion of the experiment. To evaluate the effects of MB alone, a mixture of 10 µl Optison and 50 µl PBS was injected into the tumor, which was irradiated ultrasonically and measured for size as before. Each group in the above experiment contained two mice.

Immunostaining. Bleomycin was chelated with iron that was present in the cell, and reactive oxygen species (ROS) were refined as described.[29,30] When iron binds to the iron binding site within bleomycin it captures oxygen and produces a free radical (ROS) which induces an anti-tumor effect by cleaving DNA.[31,32] As a result of the ROS reaction, the production of the free radical 8OHdG within the cell nucleus was closely monitored. In order to verify that the bleomycin migrated into the cell, immunohistochemical staining was performed on extracted melanoma tumor tissue using the mouse 8OHdG polyclonal antibody (Nikken SEIL, Shizuoka, Japan). The immunostaining protocol was performed according to the method of Hattori et al.[33] 8OHdG is also observed in apoptosis during tumor proliferation. Therefore, tumors of 4 mm diameter were injected with bleomycin alone or in conjunction with ultrasonic irradiation or injected with bleomycin and MB in conjunction with ultrasonic irradiation. The mice were then euthanized, the tumors extracted and embedded in paraffin, then sliced into 5-µm sections, immunostained, and examined by fluorescence microscopy (BX51, Olympus, Tokyo, Japan). The control was defined as a tumor extracted when it had reached 4 mm in diameter before rapid enlargement.

Drug localization. Drug localization was performed using FITC-dextran (FD-4, which has the molecular weight closest to that of bleomycin). FD-4 was diluted in PBS and adjusted to 10 mg/ml. Tumors were injected with 50 µl of FD-4 alone (n = 4), or with 50 µl FD-4 mixed with 10 µl MB in combination with ultrasonic irradiation (n = 4). Ultrasound was irradiated at 2 W/cm^2 power density, 50% duty cycle and 240 s duration. Two samples in each group were extracted 2 h and 20 h after irradiation, sliced into 6-µm sections and observed under fluorescence microscopy.

Side effects. The side effect of the present treatment was evaluated systemically and locally. The systemic effect was evaluated by histological study for various organs such as brain, lung, liver, heart on day 14. The local side effect was also evaluated by histological examination. The local temperature was also monitored by thermographic examinations.[23,34] The irradiated site temperature were calculated during ultrasonic irradiation using thermography TH6200 (NEC San-ei Instruments, Tokyo, Japan), at 2 W/cm^2 power density, 50% duty cycle and 240 second duration. In order to examine the relationship between temperature and tissue damage, the skin on the backs of SCID mice was also irradiated at 2 W/cm^2 power density, 50% duty cycle and 240 second duration, and the strongest irradiated energy of 2 W/cm^2, 100% duty cycle and 240 second duration. Twenty-four hours after the completion of the experiment, approximately 2 x 2 cm of skin from the center of the irradiated site was removed with scissors from euthanized animals and histologically examined.

Histopathological examination. After the experiment, each mouse was euthanized with an intraperitoneal overdose injection of pentobarbital sodium salt (Nembutal, 100 mg/kg), and the tumor was extracted and examined histopathologically. Samples for fluorescence microscopy and 8 OHdG immunohistological staining were fixed in formaldehyde (diluted to 3.7% with PBS), fully dewatered with alcohol, paraffin-embedded, and 5-µm sections prepared. Morphological tissue changes were examined by hematoxylin and eosin (HE) staining.

Following tumor resection, the fluorescence microscopy sample of FD-4-treated tissue was immediately frozen in liquid nitrogen and 6-µm sections prepared. FITC fluorescence was observed using a 515-nm filter.

Statistical analysis. All values were expressed as means ± standard error of the mean (SEM). Repeated measure analysis of variance (ANOVA) with a subsequent paired t test was used to determine the significance of differences in a multiple comparison. A p value of <0.05 was considered statistically significant.

RESULTS

Optimal conditions. The ultrasound conditions that would be most effective in drug delivery while avoiding extensive damage to cells were investigated. As per our previous experiment,[23] the cell count 96 h after irradiation was low (approximately 500) and cell growth was similar or significantly lower than the control under several conditions (Table 1). When the duty cycle was set at 50%, there was no significant difference in cell counts between the irradiation times of 60 or 120 s. However, cell damage was more extensive at 120 s.

Following administration of 10, 20 and 40 µl Optison, the cell count was slightly lower than the control although the differences were not significant (data not shown). When ultrasound was irradiated in conjunction with Optison, the cell count was lower at 40 µl than at 10 or 20 µl (data not shown). Experiments thereafter were performed at 1 W/cm^2, 50% duty cycle and 60 s duration, under which conditions ultrasound and MB had little effect on cell counts or growth.

Effects of bleomycin according to dosage. In the group that received a single dose of bleomycin alone at a concentration of 5 µM, the cell count at all measurement points was suppressed at around 500, which was significantly different to the control (Fig. 1A). When bleomycin was administered at concentrations of 0.5, 0.05, 0.005, 0.0005 or 0.00005 µM, the cell count and growth rate did not differ significantly from the control (Fig. 1A).

In the groups receiving bleomycin in combination with ultrasound at 5 or 0.5 µM, the cell count at each observation was suppressed at around 500, which was significantly different to the control (Fig. 1B). When bleomycin was administered at concentrations of 0.05, 0.005, 0.0005 and 0.00005 µM, there were no significant differences from the control in terms of cell count or growth rate (Fig. 1B).

In the group given a combination of MB, bleomycin and ultrasound, cell count suppression was seen at concentrations of 5, 0.5, 0.05, 0.005, 0.0005 and 0.00005 µM when 10 µl MB was administered. The cell count increased with decreasing concentrations of bleomycin (Fig. 1C). Similar results were achieved when 20 µl MB was administered (data not shown).

Evaluation of bleomycin anti-tumor effects. The anti-tumor effects of bleomycin were assessed by comparing mean relative tumor weights. The tumor was described as "enlarged" if its mean relative weight was 1 or higher, and "decreased" if it was less than 1. In the control group, the mean relative tumor weight rapidly increased throughout the experiment (Fig. 2A).

In the group administered with bleomycin only, the mean relative tumor weight increased even when the highest concentration of 2 mg/ml was administered. There was no tumor suppression effect at any of the concentrations studied. Although it was possible to slow the speed of tumor enlargement at 1 mg/ml and 2 mg/ml, the tumors resumed their rapid enlargement when bleomycin administration was stopped (data not shown). This tumor growth suppression effect decreased as the bleomycin concentration was lowered. The speed of enlargement was greatest at bleomycin concentrations of 0.5 mg/ml and 0.25 mg/ml (Fig. 2A, a).

In the group administered with bleomycin in combination with ultrasound, the mean relative tumor weight at 1 mg/ml decreased throughout the experiment (Fig. 2A, b). At 1 mg/ml and 0.5 mg/ml, the mean relative tumor weight at the completion of the experiment and afterwards decreased to 1 or less and the size of the tumor

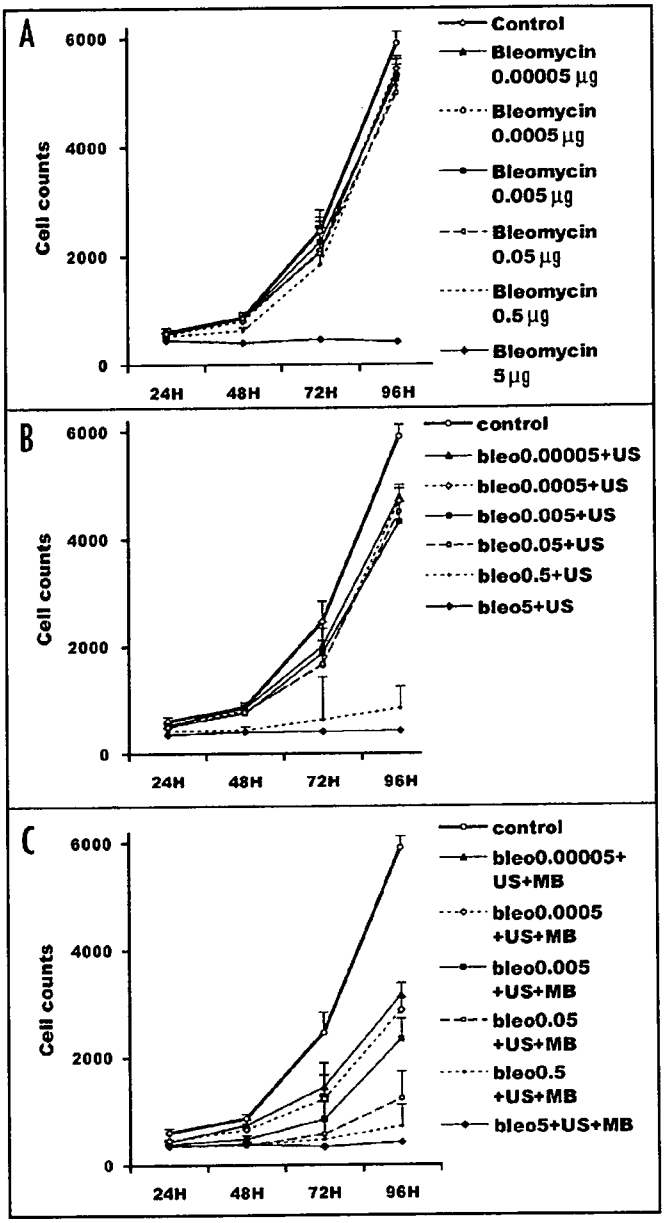

Figure 1. Effects of bleomycin according to in vitro dosage. Cell counts 24, 48, 72 and 96 h after irradiation at concentrations of 5 µM, 0.5, 0.05, 0.005, 0.0005 and 0.00005 µM were compared with controls: for (A) the group receiving a single dose of bleomycin alone (B) the group receiving ultrasound and bleomycin and (C) the group receiving a combination of Optison, bleomycin and ultrasound.

decreased (data not shown). At 0.25 mg/ml, the size of the tumor was virtually unchanged and there was no enlargement after completion of the experiment. At concentrations of 0.125 mg/ml and 0.06 mg/ml, tumors were seen to enlarge to a moderate degree. Although tumor shrinkage was not observed as a result of bleomycin treatment alone at any concentration, significant shrinkage was noted when ultrasound was combined with bleomycin treatment, even at low concentrations of bleomycin.

In the group administered with a combination of bleomycin, ultrasound and MB, there was clear tumor shrinkage at concentrations

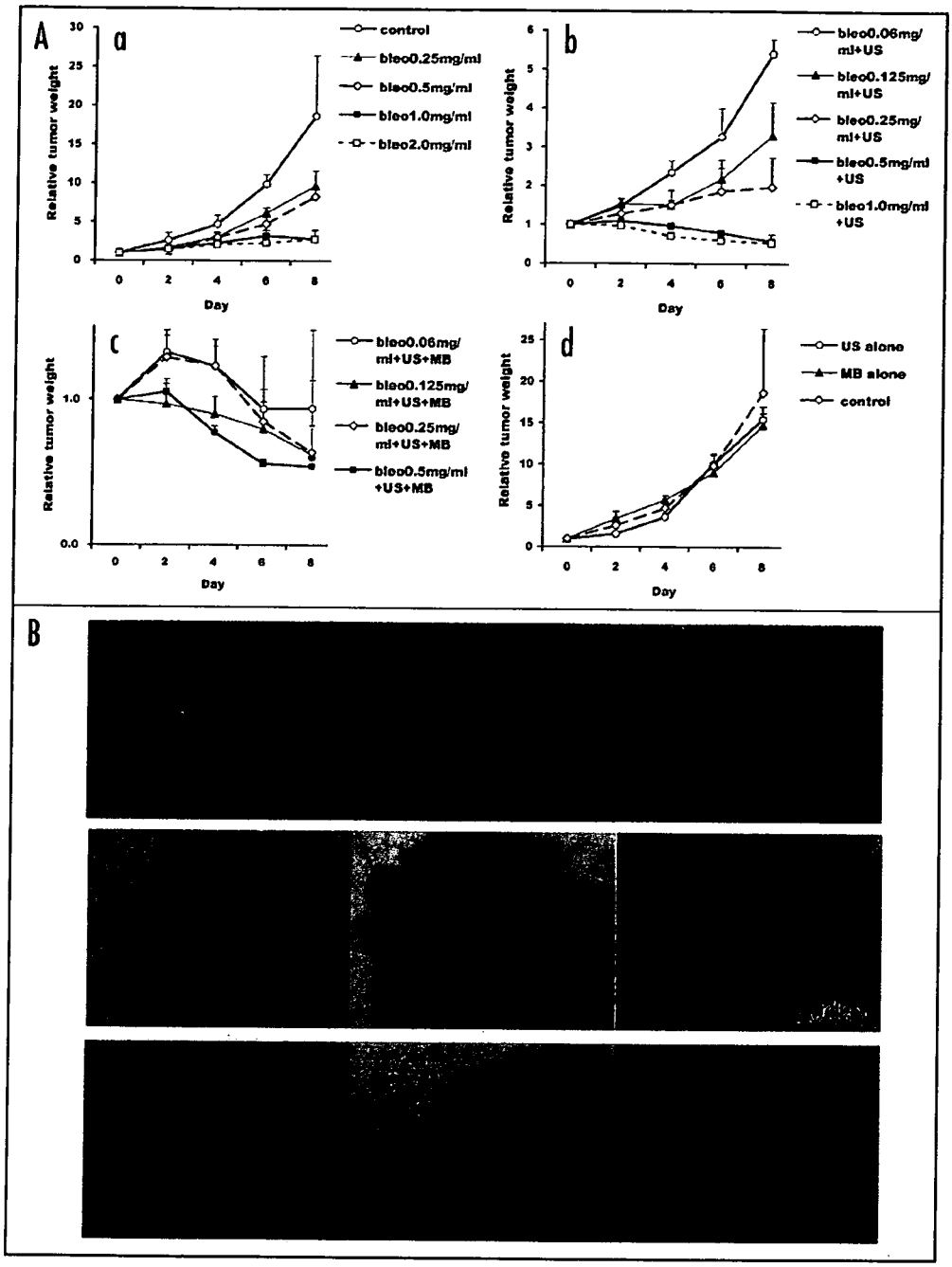

Figure 2. Anti-tumor effects of bleomycin in the malignant melanoma mouse model. (A). The anti-tumor effects of bleomycin were assessed by comparing the mean relative tumor weight of controls with (a) the group administered bleomycin only, (b) the group administered bleomycin in combination with ultrasound, (c) the group that received bleomycin in combination with ultrasound and MB, and (d) the groups receiving either ultrasonic irradiation or MB treatment alone. (B) Examples of the visual observation of tumor growth in the mouse model. A representative animal from each of the groups treated with (a) bleomycin only, (b) bleomycin in combination with ultrasound and MB and (c) ultrasound only is shown. The left panel shows the mice at day 0, when the tumor diameter had reached 4–5 mm, the middle panel after four days, right panel after ten days.

of 0.5 mg/ml (Fig. 2A, c). At 0.25 mg/ml, tumors gradually enlarged but did not increase further after the completion of the experiment. At 0.125 mg/ml and 0.06 mg/ml, tumor enlargement took place, but at a slow rate compared to the control. Thus, when MB were included in the treatment, the extent of tumor shrinkage was greater than that achieved using ultrasound alone at the same concentrations of bleomycin (Fig. 2B).

Evaluation of ultrasound/MB anti-tumor effects. In the groups receiving ultrasonic irradiation or MB treatment alone, no tumor shrinkage was observed and there was no significant difference in terms of cell counts or growth rates from the control (Fig. 2A, d).

Immunostaining. A large number of cells stained positive for 8 OHdG in the group administered with bleomycin in combination with ultrasound, and MB (Fig. 3B) and in the group administered with bleomycin in combination with ultrasound (data not shown). Comparatively few cells in the control group stained positive for 8OHdG (Fig. 3A). The results of immunostaining were consistent with findings within the tumor cell nuclei.

FITC-dextran. Strong, uniform fluorescence of the tumor cell nucleus and cytoplasm and peripheral tissue was observed after 2 h in the FD-4 injection only group, the ultrasound only group, and the ultrasound/MB combined group (Fig. 4A). After 20 h, virtually no fluorescence was seen in the injection only group (Fig. 4B). Strong, patchy fluorescence remained in the ultrasound group and ultrasound/MB group, which was particularly strong on the side of the tumor that had received ultrasound irradiation (Fig. 4C).

Side effects. After the irradiation of ultrasound of 2 W/cm^2 power density, 50% duty cycle, and 240 second duration, the local temperature increased from 34–37°C immediately after irradiation, and remained at 37°C constantly thereafter. The temperature of the probe showed similar changes. Ultrasound irradiation of the backs of SCID mice at 2 W/cm^2 power density, 50% duty cycle, and 240 second duration showed similar results to tumor irradiation, and there were no particular abnormalities in the external appearance during extirpation. At the time of excision, the skin appeared slightly reddish in several places. Hematoxylin and eosin staining of the

excised tissue revealed no abnormalities in the tissue exposed to ultrasound of the duty cycle set at 50%. While, when it came to 100%, some of the epithelial cells were found to have disappeared or the epidemis looked thinned. The histological examination of brain, lung, liver or heart on day 14. The results showed no abnormalities such as inflammation or degeneration in any tissues (data not shown).

Histological examination. In the control group, HE staining revealed active cell division, nuclear heteromorphism and pigmentation, and active proliferation of melanoma cells (Fig. 5A). In the tissue of tumors that had been reduced in size, only a small amount of tumor cells remained in the deepest part of the tumor. This was the case for tumors in the two groups treated with bleomycin in combination with ultrasound, and with ultrasound and MB. Most of these remaining tumor cells had necrotized (Fig. 5B). In cases where tumor enlargement was seen, those groups in which the speed of tumor growth was slower than the control also showed necrosis. The ultrasound only group and MB only group did not differ greatly from the control group, and no abnormalities were seen in the tissue at nontumor sites.

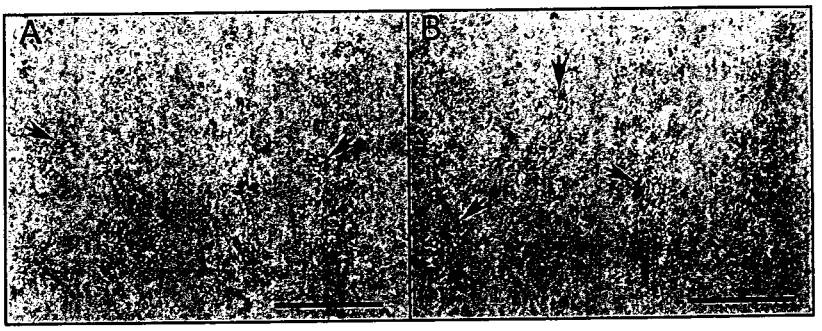

Figure 3. Immunohistochemical staining of the melanoma tumor tissue using the mouse 8 OHdG polyclonal antibody. Arrows indicate cells staining positive for 8 OHdG in (A) the control group and (B) the group administered with bleomycin, ultrasound (irradiation conditions: 2 W/cm^2 power density, 50% duty cycle and 240 sec duration) and MB. Bar, 50 μm.

DISCUSSION

The present study shows that the inhibitory effect of bleomycin on the growth of B-16 cells was significantly enhanced in vitro after ultrasound irradiation alone and when ultrasound irradiation was combined with MB administration. In vivo results showed that following the administration of 2.0 mg/ml bleomycin alone tumors continued to become enlarged gradually, but when bleomycin treatment, even at a concentration of 0.25 mg/ml, was combined with ultrasound, the growth in size of most tumors was arrested. Furthermore, when bleomycin, ultrasound irradiation, and MB were administered concomitantly, tumors decreased in size, even at the low bleomycin dose of 0.06 mg/ml. The same effect as bleomycin treatment alone was therefore achieved at 1/8 the concentration when ultrasound was included, and at a remarkable 1/33 concentration when both ultrasound and MB were used in combination.

Low-energy ultrasound has recently been highlighted as a drug/gene transfer method, but it is unclear why in the present experiment a tumor suppressive effect was enhanced by ultrasound irradiation, and why this effect was further enhanced by adding MB.[5,7,20] In our experiment, tumor suppression was not seen in a control group whose tumors were only irradiated with ultrasound, or in a control group administered with MB alone. The temperature of the irradiated site was 37°C (data not shown), so it is unlikely that the tumor suppression effect was due to the heat of the ultrasound or to a harmful effect of the MB.

Previous reports have demonstrated that small, reversible openings form in the cell membrane due to a cavitation effect caused by low-energy ultrasound irradiation.[35,36] Furthermore, it is known that because MB are similar to the vesicles present during cavitation, a similar effect to ultrasound irradiation occurs, even at lower energy levels.[21,24] MB liquid microjets initiated by rupture from the ultrasound cause small openings to form in the cell membrane. We therefore examined whether ultrasound (alone or in combination with microbubbles) accentuated the intracellular uptake and

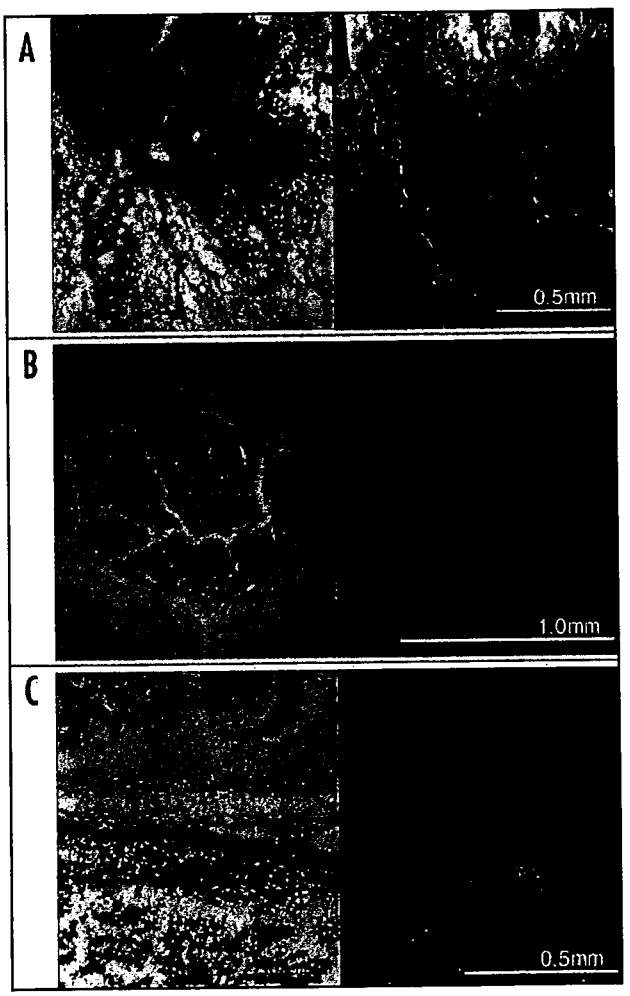

Figure 4. FITC-dextran. Fluorescence microscopy images after FD-4 in (A) the FD-4 only injection group after 2 h, (B) the FD-4 only injection group after 20 h and (C) the ultrasound ultrasound/MB group after 20 h. The right panel shows that the fluorescence in this group was particularly strong on the side of the tumor that had received ultrasound irradiation. Asterisks indicate the side of the tumor.

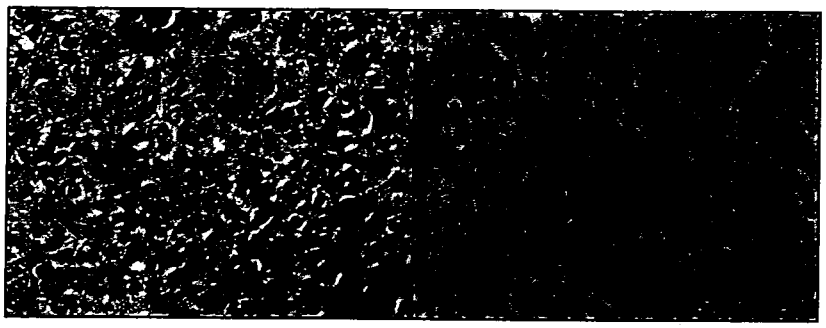

Figure 5. HE staining of extracted tumor tissue. HE staining of tumor tissue samples from (A) the control group and (B) the group treated with bleomycin, ultrasound and MB. Tumor cells are indicated by arrows. Active cell division, nuclear heteromorphism, and pigmentation are evident. Bar, 50 μm.

pharmacological effects of bleomycin. FITC-dextran (FD-4, MW 4000) was used, as we could not directly observe bleomycin.

Our results showed that 20 h after injection of FD-4 alone, virtually no fluorescence remained. When ultrasound and Optison were combined with FD-4 injection, extensive intracellular fluorescence remained 20 h after treatment. That FITC fluorescence was observed throughout the entire cell suggests that dextran entered the cell nonselectively through the cell membrane rather than through selective phagocytosis.

Next, we examined changes that occurred after bleomycin entered the cell. Bleomycin damages DNA by entering the cell nucleus and chelating with iron, thereby producing ROS.[29,31,32] Using this knowledge, immunostaining for 8O HdG was performed to measure damage.[33] The results revealed a high level of positive staining in the cell nuclei in the groups treated with bleomycin and ultrasound only and with ultrasound and MB combined. In contrast, 8OHdG was virtually unseen in the control group and the group administered with bleomycin alone. Although these results provide only indirect proof, they suggest that ultrasound and MB introduce bleomycin into the cell at a high rate, thus producing a pharmacological effect. These findings are consistent with experimental results previously reported.[13,14,17]

Also of note is that the localization of FD-4 and 8OHdG was observed more specifically in melanoma cells than in peripheral healthy tissue. The reason for this is unclear, although it might be that the cell membrane of tumor cells is more sensitive to ultrasound than that of noncancerous cells. Kondo et al. reported that levovist, a type of microbubble, inherently and selectively adsorbs to leukocytes.[37] If microbubbles adsorb to malignant melanoma cells in the same way, this could provide an explanation for the localization of FD-4 and 8 OHdG. This idea is currently under investigation.

In the present study, the ultrasound was not strongly cytopathic in B-16 cells at 1 W/cm^2 power density, 50% duty cycle, and a duration of 120 s or less or at 2 W/cm^2 power density, 50% duty cycle and a duration of 120 s or less. There were also no histological abnormalities in tumor peripheral tissue, and the irradiated site did not reach a high temperature (data not shown).

It is not clear whether the same therapeutic effects would be obtained in humans as observed in the mouse experiment, but we do not anticipate any major problems in clinical applications using the tools and conditions tested in the current study. In the treatment of large facial tumors, cosmetic problems can arise after surgery, even when a tumor is resected. It would therefore be extremely beneficial to resect the tumor after reducing its size using the present method.

In conclusion, the anti-tumor effect of bleomycin on B-16 melanoma cells was enhanced by low-energy ultrasound that was not harmful to tissue. By combining this treatment with microbubbles, the effect was further enhanced and tumor growth was inhibited even at a low concentration of the drug. A nonthermal effect of low energy ultrasound could be an effective method for treating cancer. In particular, it could enable dosages of anticancer drugs to be lowered, and ameliorate adverse reactions. Moreover, the indication that microbubbles are a potentially useful tool for drug delivery should lead to the development of new transfer methods.

References

1. Reddy LH. Drug delivery to tumours: Recent strategies. J Pharm Pharmacol 2005; 57:1231-42.
2. Nechushtan H, Peretz T. Tamoxifen and breast cancer. Harefuah 2002; 141:718-20, 61, 60.
3. Madersbacher S, Pedevilla M, Vingers L, Susani M, Marberger M. Effect of high-intensity focused ultrasound on human prostate cancer in vivo. Cancer Res 1995; 55:3346-51.
4. Unger EC, Hersh E, Vannan M, Matsunaga TO, McCreery T. Local drug and gene delivery through microbubbles. Prog Cardiovasc Dis 2001; 44:45-54.
5. Tachibana K, Tachibana S. Application of ultrasound energy as a new drug delivery system. Nippon Rinsho 1998; 56:584-8.
6. Tachibana K, Tachibana S. The use of ultrasound for drug delivery. Echocardiography 2001; 18:323-8.
7. Lindner JR, Kaul S. Delivery of drugs with ultrasound. Echocardiography 2001; 18:329-37.
8. Larina IV, Evers BM, Esenaliev RO. Optimal drug and gene delivery in cancer cells by ultrasound-induced cavitation. Anticancer Res 2005; 25:149-56.
9. Mohamed MM, Mohamed MA, Fikry NM. Enhancement of antitumor effects of 5-fluorouracil combined with ultrasound on Ehrlich ascites tumor in vivo. Ultrasound Med Biol 2003; 29:1635-43.
10. Marmor JB, Hilerio FJ, Hahn GM. Tumor eradication and cell survival after localized hyperthermia induced by ultrasound. Cancer Res 1979; 39:2166-71.
11. Cheung AY, Neyzari A. Deep local hyperthermia for cancer therapy: External electromagnetic and ultrasound techniques. Cancer Res 1984; 44:4736s-44s.
12. Chapelon JY, Margonari J, Vernier F, Gorry F, Ecochard R, Gelet A. In vivo effects of high-intensity ultrasound on prostatic adenocarcinoma Dunning R3327. Cancer Res 1992; 52:6353-7.
13. Tachibana K, Uchida T, Tamura K, Eguchi H, Yamashita N, Ogawa K. Enhanced cytotoxic effect of Ara-C by low intensity ultrasound to HL-60 cells. Cancer Lett 2000; 149:189-94.
14. Nelson JL, Roeder BL, Carmen JC, Roloff F, Pitt WG. Ultrasonically activated chemotherapeutic drug delivery in a rat model. Cancer Res 2002; 62:7280-3.
15. Tomizawa M, Ebara M, Saisho H, Sakiyama S, Tagawa M. Irradiation with ultrasound of low output intensity increased chemosensitivity of subcutaneous solid tumors to an anti-cancer agent. Cancer Lett 2001; 173:31-5.
16. Yuh EL, Shulman SG, Mehta SA, Xie J, Chen L, Frenkel V, Bednarski MD, Li KC. Delivery of systemic chemotherapeutic agent to tumors by using focused ultrasound: Study in a murine model. Radiology 2005; 234:431-7.
17. Miller DL, Pislaru SV, Greenleaf JE. Sonoporation: Mechanical DNA delivery by ultrasonic cavitation. Somat Cell Mol Genet 2002; 27:115-34.
18. Miller DL, Bao S, Gies RA, Thrall BD. Ultrasonic enhancement of gene transfection in murine melanoma tumors. Ultrasound Med Biol 1999; 25:1425-30.
19. Taniyama Y, Tomita N, Endoh S, Kaneda Y, Ogihara T, Morishita R. Gene transfer with ultrasound and microbubbles (optison) as a potential treatment for cardiovascular diseases. Nippon Ronen Igakkai Zasshi 2004; 41:51-4.
20. Dijkmans PA, Juffermans LJ, Musters RJ, van Wamel A, ten Cate FJ, van Gilst W, Visser CA, de Jong N, Kamp O. Microbubbles and ultrasound: From diagnosis to therapy. Eur J Echocardiogr 2004; 5:245-56.
21. Feinstein SB. The powerful microbubble: From bench to bedside, from intravascular indicator to therapeutic delivery system, and beyond. Am J Physiol Heart Circ Physiol 2004; 287: H450-7.

22. Lindner JR. Evolving applications for contrast ultrasound. Am J Cardiol 2002; 90:72J-80J.
23. Sonoda S, Tachibana K, Uchino E, Okubo A, Yamamoto M, Sakoda K, Hisatomi T, Sonoda KH, Negishi Y, Izumi Y, Takao S, Sakamoto T. Gene transfer to corneal epithelium and keratocytes mediated by ultrasound with microbubbles. Invest Ophthalmol Vis Sci 2006; 47:558-64.
24. Greenleaf WJ, Bolander ME, Sarkar G, Goldring MB, Greenleaf JF. Artificial cavitation nuclei significantly enhance acoustically induced cell transfection. Ultrasound Med Biol 1998; 24:587-95.
25. Tsutsui JM, Xie F, Porter RT. The use of microbubbles to target drug delivery. Cardiovasc Ultrasound 2004; 2:23.
26. Rapoport NY, Christensen DA, Fain HD, Barrows L, Gao Z. Ultrasound-triggered drug targeting of tumors in vitro and in vivo. Ultrasonics 2004; 42:943-50.
27. Larina IV, Evers BM, Ashitkov TV, Bartels C, Larin KV, Esenaliev RO. Enhancement of drug delivery in tumors by using interaction of nanoparticles with ultrasound radiation. Technol Cancer Res Treat 2005; 4:217-26.
28. Ovejera AA, Houchens DP, Barker AD. Chemotherapy of human tumor xenografts in genetically athymic mice. Ann Clin Lab Sci 1978; 8:50-6.
29. Hara N, Ichinose Y, Motohiro A, Kuda T, Aso H, Ohta M. Influence of chemotherapeutic agents on superoxide anion production by human polymorphonuclear leukocytes. Cancer 1990; 66:684-8.
30. Masuda H, Tanaka T, Takahama U. Cisplatin generates superoxide anion by interaction with DNA in a cell-free system. Biochem Biophys Res Commun 1994; 203:1175-80.
31. Goto M, Koga N, Ohse Y, Kurosaki H, Komatsu T, Kuroda Y. Dependence of dehydrogenation of amines towards coordination geometry - Oxidation-products of Tricyano[Di(2-Pyridylmethyl)Amine]ferrate from Mer and Fac Isomers. J Chem Soc Chem Comm 1994; 2015-6.
32. Ishikawa Y, Morishita Y, Yamamoto T, Kurosaki H, Goto M, Matsuo H, Sugiyama M. Oxidative and random cleavage of DNA by the novel iron(II) complex capable of yielding an iron(III) hydroperoxide intermediate. Chem Lett 1998; 39-40.
33. Hattori Y, Nishigori C, Tanaka T, Uchida K, Nikaido O, Osawa T, Hiai H, Imamura S, Toyokuni S. 8-hydroxy-2'-deoxyguanosine is increased in epidermal cells of hairless mice after chronic ultraviolet B exposure. J Invest Dermatol 1996; 107:733-7.
34. Sakamoto T, Oshima Y, Sakamoto M, Kawano YI, Ishibashi T, Inomata H, Ohnishi Y. Electroporation and bleomycin in glaucoma-filtering surgery. Invest Ophthalmol Vis Sci 1997; 38:2864-8.
35. Tachibana K, Uchida T, Hisano S, Morioka E. Eliminating adult T-cell leukaemia cells with ultrasound. Lancet 1997; 349:325.
36. Taniyama Y, Tachibana K, Hiraoka K, Namba T, Yamasaki K, Hashiya N, Aoki M, Ogihara T, Yasufumi K, Morishita R. Local delivery of plasmid DNA into rat carotid artery using ultrasound. Circulation 2002; 105:1233-9.
37. Kondo I, Ohmori K, Oshita A, Takeuchi H, Yoshida J, Shinomiya K, Fuke S, Suzuki T, Mizushige K, Kohno M. Leukocyte-targeted myocardial contrast echocardiography can assess the degree of acute allograft rejection in a rat cardiac transplantation model. Circulation 2004; 109:1056-61.